7

Strip Gratings and Other Two-Dimensional Structures with One-Dimensional Periodicity

Periodic structures find applications as electromagnetic filters, polarizers, artificial dielectrics, and radomes. These scatterers are electrically large and would be intractable if not for the fact that the computational domain can be restricted to one period of the geometry. Integral equation formulations from the preceding chapters can be systematically extended to periodic scatterers through the use of periodic Green's functions. The development of these functions is most easily understood through Fourier transforms, and we begin by reviewing elementary properties of Fourier integrals. In their original form, periodic Green's functions give rise to slowly converging summations that must be evaluated during method-of-moments analysis. Several approaches for accelerating the slowly converging summations will be considered. After illustrating several specific integral equation formulations, this chapter concludes with the development of an outward-looking differential equation formulation for inhomogeneous gratings.

7.1 FOURIER ANALYSIS OF PERIODIC FUNCTIONS [1]

The Fourier transform can be defined in several ways. For the purpose of this chapter, the transform and its inverse will be defined as

$$F\{A(x)\} = \tilde{A}(f) = \int_{-\infty}^{\infty} A(x)e^{-j2\pi fx}\,dx \tag{7.1}$$

and

$$F^{-1}\{\tilde{A}(f)\} = A(x) = \int_{-\infty}^{\infty} \tilde{A}(f)e^{j2\pi fx}\,df \tag{7.2}$$

The convolution of two functions is the operation defined by

$$A(x) * B(x) = \int_{-\infty}^{\infty} A(x')B(x - x')\,dx' \tag{7.3}$$

We have seen that convolutions arise naturally in integral equation formulations (Chapter 5). The convolution theorem associated with the Fourier transform states that

$$A(x) * B(x) = F^{-1}\{\tilde{A}(f)\tilde{B}(f)\} \tag{7.4}$$

An alternative form of the convolution theorem states that

$$A(x)B(x) = F^{-1}\{\tilde{A}(f) * \tilde{B}(f)\} \tag{7.5}$$

Thus, Fourier transforms offer an alternative way of evaluating a convolution integral. This property is especially useful when the functions involved are discrete or periodic.

A periodic function $A_p(x)$ may be constructed from the convolution operation

$$A_p(x) = A(x) * P(x) \tag{7.6}$$

where $A(x)$ is an arbitrary function and $P(x)$ is the "comb" function, defined as

$$P(x) = \sum_{i=-\infty}^{\infty} \delta(x - i\,\Delta X) \tag{7.7}$$

Performing the convolution operation yields the function

$$A_p(x) = \sum_{i=-\infty}^{\infty} A(x - i\,\Delta X) \tag{7.8}$$

which is periodic with period ΔX (Figure 7.1).

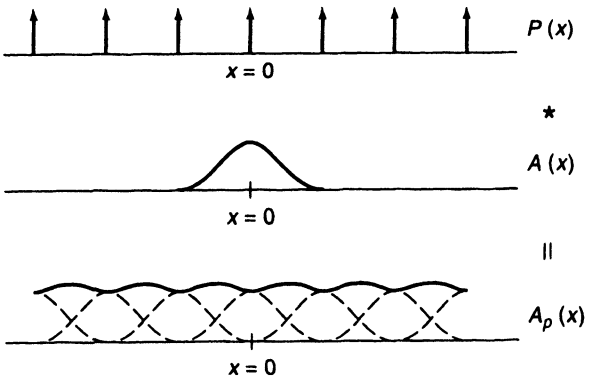

Figure 7.1 Convolution with a comb function.

The Fourier transform of the comb function $P(x)$ is another comb function

$$\tilde{P}(f) = \Delta f \sum_{i=-\infty}^{\infty} \delta(f - i\,\Delta f) \tag{7.9}$$

where

$$\Delta f = \frac{1}{\Delta X} \tag{7.10}$$

Using the convolution theorem, the transform of $A_p(x)$ can be obtained as

$$\tilde{A}_p(f) = \tilde{A}(f)\tilde{P}(f) = \Delta f \sum_{i=-\infty}^{\infty} \tilde{A}(i\Delta f)\delta(f - i\Delta f) \tag{7.11}$$

Multiplication with the comb function $\tilde{P}(f)$ is equivalent to a sampling operation, and the transform $\tilde{A}_p(f)$ is a discrete function. The Fourier transform of any periodic function is discrete, with the period and sampling interval related by Equation (7.10).

A discrete function $A_d(x)$ can be constructed by sampling a function $A(x)$ at regular intervals of Δx (Figure 7.2). This process, which can be expressed as multiplication with the comb function

$$S(x) = \sum_{i=-\infty}^{\infty} \delta(x - i\,\Delta x) \tag{7.12}$$

produces

$$A_d(x) = A(x)S(x) = \sum_{i=-\infty}^{\infty} A(i\,\Delta x)\delta(x - i\,\Delta x) \tag{7.13}$$

The Fourier transform of $S(x)$ is the comb function

$$\tilde{S}(f) = \Delta F \sum_{i=-\infty}^{\infty} \delta(f - i\,\Delta F) \tag{7.14}$$

where ΔF is related to the sampling interval Δx by

$$\Delta F = \frac{1}{\Delta x} \tag{7.15}$$

The convolution theorem of Equation (7.5) can be employed to produce the transform

$$\tilde{A}_d(f) = \tilde{A}(f) * \tilde{S}(f) = \Delta F \sum_{i=-\infty}^{\infty} \tilde{A}(f - i\,\Delta F) \tag{7.16}$$

The function $\tilde{A}(f)$ is periodic with period ΔF. We see that the Fourier transform of a discrete function is periodic, with period and sampling interval related by Equation (7.15).

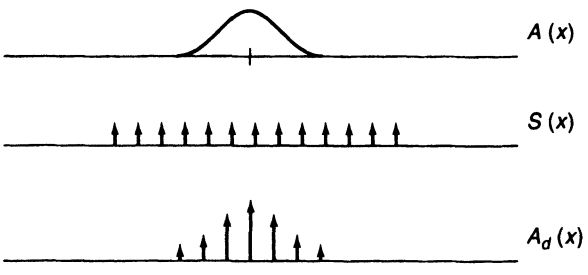

Figure 7.2 Sampling with a comb function.

Ultimately, numerical evaluation may require the discretization of both the original and transform domains. A representation that is both discrete and periodic can be obtained

by the expression

$$A_{dp}(x) = [A(x) * P(x)]\, S(x) \tag{7.17}$$

which has the Fourier transform

$$\tilde{A}_{dp}(f) = \left[\tilde{A}(f) * \tilde{S}(f)\right] \tilde{P}(f) \tag{7.18}$$

Thus, the transform of a discrete, periodic function is itself discrete and periodic. For these functions, Fourier transforms reduce to discrete Fourier transforms and their exact implementation can be obtained using the fast Fourier transform (FFT) algorithm.

7.2 FLOQUET HARMONICS [2]

The cross-sectional view of a strip grating is illustrated in Figure 7.3. This two-dimensional geometry is an infinite periodic extension of a "unit cell" containing a single strip, also illustrated in the figure. The precise location of the unit cell is arbitrary, and it may straddle two strips or even contain more than one complete strip, provided that its periodic repetition reproduces the original structure. We wish to determine the electromagnetic response of the strip grating due to a plane-wave excitation of the form

$$E_z^{\text{inc}}(x, y) = E_0 e^{-jk(x\cos\theta + y\sin\theta)} \tag{7.19}$$

This uniform plane wave is a special case of a general excitation satisfying the condition

$$E_z^{\text{inc}}(x + a, y) = E_z^{\text{inc}}(x, y) e^{-jk_x a} \tag{7.20}$$

where a is the dimension of the unit cell of Figure 7.3 and $k_x a$ represents a linear progressive phase shift from one unit cell to the next.

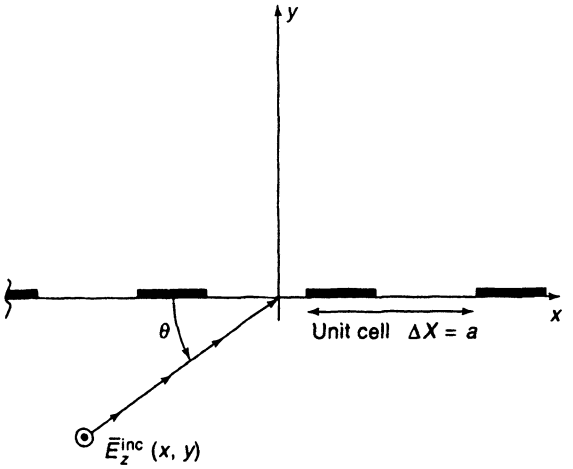

Figure 7.3 Periodic strip grating.

The electromagnetic response to such an excitation can be expressed as a superposition of Floquet harmonics,

$$E_z^s(x, y) = \sum_{n=-\infty}^{\infty} e_n \Psi_n(x, y) \tag{7.21}$$

where

$$\Psi_n(x, y) = e^{-jk_{xn}x} e^{\pm j\sqrt{k^2 - k_{xn}^2}\,y} \tag{7.22}$$

and

$$k_{xn} = k_x - \frac{2\pi}{a} n \tag{7.23}$$

When $k^2 > k_{xn}^2$, Floquet harmonics are waves that propagate away from the grating [the plus or minus sign in (7.22) is used when $y < 0$ or $y > 0$, respectively]. When $k_{xn}^2 > k^2$, the branch of the square root is taken to ensure that the harmonics decay in a direction away from the grating.

The Floquet harmonics form a complete orthogonal set over one period of the geometry in x and preserve the desired progressive phase shift imposed by the excitation for all x. Some of the terms in the expansion represent waves that exhibit true propagation (i.e., the visible region $k_{xn}^2 < k^2$) while others represent evanescent waves (the invisible region $k_{xn}^2 > k^2$). Of the infinite number of Floquet harmonics, generally only a few are associated with true propagation. The set of Floquet harmonics is entirely determined by the geometric period and the assumed phase progression along x and thus does not depend on the specific dimensions of the strips in the grating. The coefficients $\{e_n\}$ in Equation (7.21), however, depend on the specific strip geometry.

As an illustration, Figure 7.4 shows the propagating Floquet harmonics for an example involving a wave incident 30° from normal upon a strip grating having a period equal to two wavelengths.

n	k_{xn}	k_{yn}
−1	k	0
0	$k/2$	$k\sqrt{3}/2$
1	0	k
2	$-k/2$	$k\sqrt{3}/2$
3	$-k$	0

$$k_{xn} = k\left(\cos\theta^{\text{inc}} - \frac{n}{2}\right)$$

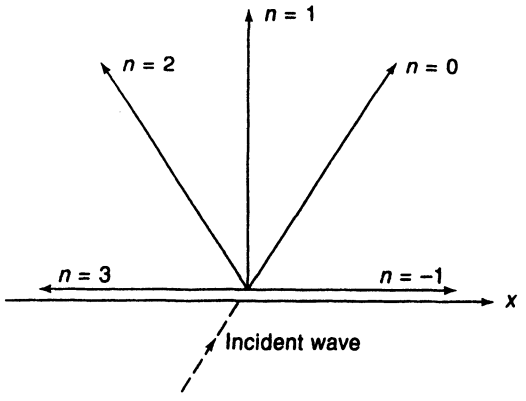

Figure 7.4 Illustration of the propagating Floquet harmonics for a grating with $\theta^{\text{inc}} = 60°$ and $a = 2\lambda_0$.

Because of the phase shift imposed by the incident field, the fields and currents of interest are not strictly periodic functions of x. Instead, they are modulated periodic functions of the general form

$$A_{mp}(x) = \sum_{i=-\infty}^{\infty} A(x - i\,\Delta X)e^{-jk_x i\,\Delta X} \tag{7.24}$$

where $\Delta X = a$. Properties of the Fourier transform dictate that

$$\tilde{A}_{mp}(f) = \tilde{A}(f)\tilde{P}(f + f_0) = \Delta f \sum_{i=-\infty}^{\infty} \tilde{A}(i\,\Delta f - f_0)\delta(f - i\,\Delta f + f_0) \tag{7.25}$$

where Δf is defined in Equation (7.10) and

$$f_0 = \frac{k_x}{2\pi} \tag{7.26}$$

As a consequence of the modulation, the transform of (7.24) is sampled at values of the transform variable f that are shifted from those of Equation (7.11).

Every periodic geometry can be associated with a *spatial lattice* of points in the original domain and a *reciprocal lattice* in the Fourier transform domain [2–4]. The spatial lattice–reciprocal lattice concept is often useful in multidimensional applications, because of the ease with which the propagating harmonics can be identified. In this trivial one-dimensional example, the strip grating imposes a lattice in x defined by the values

$$x = i\,\Delta X \tag{7.27}$$

The reciprocal lattice in the transform domain identifies the discrete spectral frequencies associated with the Floquet harmonics. These frequencies are given by the values

$$f = i\,\Delta f = \frac{i}{\Delta X} \tag{7.28}$$

For the example depicted in Figure 7.4, the spatial lattice is defined by values of x in the set $\{\ldots, -2, 0, 2, 4, 6, \ldots\}$, and the reciprocal lattice is defined by values of f in the collection $\{\ldots, -1, -\frac{1}{2}, 0, \frac{1}{2}, 1, \ldots\}$. The range $(k_x/2\pi - 1) < f < (k_x/2\pi + 1)$ defines the "visible region" of the spectrum containing the propagating Floquet harmonics (the five propagating Floquet harmonics presented in Figure 7.4 span this range).

7.3 TM SCATTERING FROM A CONDUCTING STRIP GRATING: EFIE DISCRETIZED WITH PULSE BASIS FUNCTIONS AND DELTA TESTING FUNCTIONS

Consider a TM plane wave having the form of Equation (7.19) incident on the infinite, periodic strip grating illustrated in Figure 7.3. The surface equivalence principle (Chapter 1) can be used to replace the perfect conducting strips by an equivalent electric current density $J_z(x)$. Due to the phase progression imposed by the incident field, the equivalent currents must satisfy the Floquet condition

$$J_z(x + a) = J_z(x)e^{-jk_x a} \tag{7.29}$$

A conventional EFIE formulation requires the superposition of the fields of each of the currents. If $J_z(x)$ is considered nonzero only when x is located on one of the conducting

strips, the EFIE can be written as

$$E_z^{\text{inc}}(x,0) = jk\eta \int_{-\infty}^{\infty} J_z(x') \frac{1}{4j} H_0^{(2)}(k\,|x-x'|)\,dx' \tag{7.30}$$

where the equality holds only for values of x on the conducting strips. Since the currents from one strip to the next are related by (7.29), the domain of the integral operator can be transformed to a single unit cell to produce the equivalent equation

$$E_z^{\text{inc}}(x,0) = jk\eta \int_{\text{single strip}} J_z(x') G_p(x-x')\,dx' \tag{7.31}$$

where

$$G_p(x) = \frac{1}{4j} \sum_{i=-\infty}^{\infty} H_0^{(2)}(k\,|x-ia|) e^{-jik_x a} \tag{7.32}$$

The conventional free-space Green's function employed in Equation (7.30) has been replaced by its periodic counterpart. The periodic Green's function G_p differs from the Green's functions employed in previous chapters in one fundamental way: It depends on the progressive phase shift imposed by the incident field. In other words, changes in the direction of the incident plane wave will alter both sides of Equation (7.31).

By restricting the domain of the equation to a single unit cell, the electrical size of the problem has been reduced to manageable proportions. The method-of-moments discretization of the EFIE follows in the usual manner. Suppose that the conducting strip contained in the unit cell is divided into N intervals over which pulse basis functions reside. Dirac delta testing functions can be located in the center of each interval. The resulting matrix has the general form

$$\begin{bmatrix} Z_{11} & Z_{12} & \cdots & Z_{1N} \\ Z_{21} & Z_{22} & \cdots & Z_{2N} \\ \cdot & & & \cdot \\ \cdot & \ddots & & \cdot \\ \cdot & & & \cdot \\ Z_{N1} & Z_{N2} & \cdots & Z_{NN} \end{bmatrix} \begin{bmatrix} j_1 \\ j_2 \\ \cdot \\ \cdot \\ \cdot \\ j_N \end{bmatrix} = \begin{bmatrix} e_1^i \\ e_2^i \\ \cdot \\ \cdot \\ \cdot \\ e_N^i \end{bmatrix} \tag{7.33}$$

where

$$Z_{mn} = jk\eta \int_{\text{cell } n} G_p(x_m - x')\,dx' \tag{7.34}$$

and

$$e_m^i = E_0 e^{-jk_x x_m} \tag{7.35}$$

The task of computing the entries is complicated by the slowly converging nature of the summation for G_p, and the following sections discuss this calculation. Once the matrix is obtained, Equation (7.33) can be solved to produce the coefficients of the pulse expansion for $J_z(x)$.

After the coefficients of the current density on the strips have been determined, the scattered field can be expressed in terms of the Floquet harmonics. To determine the coefficients $\{e_n\}$ in Equation (7.21), observe that since the incident field is continuous across the grating,

$$J_z(x) = H_x^s(x, 0^-) - H_x^s(x, 0^+) \tag{7.36}$$

By combining (7.21), (7.22), (7.36), and

$$H_x(x, y) = \frac{-1}{j\omega\mu}\frac{\partial E_z}{\partial y} \tag{7.37}$$

the current density can be expressed in terms of the Floquet harmonics as

$$J_z(x) = \frac{-2}{k\eta}\sum_{n=-\infty}^{\infty} e_n\sqrt{k^2 - k_{xn}^2}\,e^{-jk_{xn}x} \tag{7.38}$$

Using the orthogonality of the Floquet harmonics, the coefficients are

$$e_n = \frac{-k\eta}{2a\sqrt{k^2 - k_{xn}^2}}\int_0^a J_z(x)e^{jk_{xn}x}\,dx \tag{7.39}$$

Reflection and transmission coefficients can be defined by the ratio of the total electric field carried by the zero-order Floquet harmonic to the incident electric field (see Section 7.9). Assuming a common reference plane located at $y = 0$, these have the form

$$R_0 = \frac{e_0}{E_0} \tag{7.40}$$

and

$$T_0 = 1 + \frac{e_0}{E_0} \tag{7.41}$$

Figure 7.5 shows a plot of the reflection coefficient for a strip grating having conducting material occupying exactly half the unit cell as a function of the unit cell size. An exact solution is available for this geometry [5, 6], and the numerical results obtained from Equation (7.33) exhibit good agreement with the exact solution.

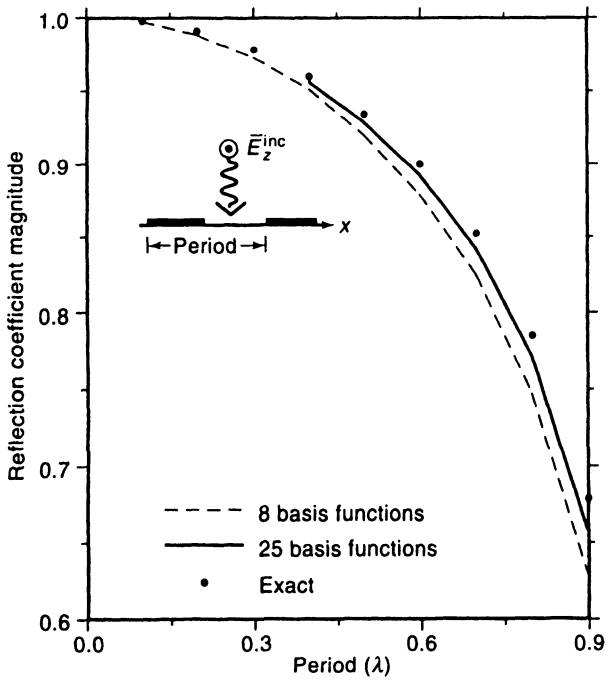

Figure 7.5 Plot of the TM reflection coefficient magnitude produced by the EFIE compared with the exact result.

7.4 SIMPLE ACCELERATION PROCEDURES FOR THE GREEN'S FUNCTION [7, 8]

The magnitude of the ith term in the periodic Green's function summation of Equation (7.32) can be estimated from the asymptotic form of the Hankel function for large arguments,

$$H_0^{(2)}(kx) \approx \sqrt{\frac{2j}{\pi kx}} e^{-jkx} \tag{7.42}$$

The ith term behaves as

$$O\left(\frac{1}{\sqrt{i}}\right) \qquad \text{as } i \to \infty \tag{7.43}$$

Obviously, the summation would diverge if not for the oscillatory behavior of the exponential function. In practice, the direct summation required in Equation (7.32) is prohibitively slow (Table 7.1 illustrates the number of terms required to produce a specified accuracy).

TABLE 7.1 Computed Decimal Places of Accuracy in $G_p(x)$

N	Using Equation (7.32)	Using Equation (7.47)	Using Equations (7.49), (7.50) with $\alpha = 0.1a$
10	1	2	3
30	1	2	4
100	1	2	4
300	1	3	4
1,000	1	3	5
3,000	2	4	5
10,000	2	4	5

Note: As a function of the upper limit N of the summation. The parameters are $a = 0.8\lambda$, $x = 0.5\lambda$, and $\theta^{\text{inc}} = 60$ deg. The correct answer is $G_p(x) \cong 0.05779617 + j\,0.13912689$.

To improve the efficiency of the calculation, we consider an acceleration technique based on the Fourier transform pair from Equations (7.1) and (7.2). This procedure is sometimes known as the *Poisson sum transformation* [7]. Using

$$F\{H_0^{(2)}(k\,|x|)\} = \frac{2}{\beta_y} \tag{7.44}$$

where

$$\beta_y = \begin{cases} \sqrt{k^2 - (2\pi f)^2} & k^2 > (2\pi f)^2 \\ -j\sqrt{(2\pi f)^2 - k^2} & k^2 < (2\pi f)^2 \end{cases} \tag{7.45}$$

the Fourier transform of $G_p(x)$ can be found from (7.25) to be

$$\tilde{G}_p(f) = \frac{1}{2ja} \sum_{i=-\infty}^{\infty} \delta\left(f - \frac{i}{a} + \frac{k_x}{2\pi}\right) \frac{1}{\beta_y} \tag{7.46}$$

Applying the inverse Fourier transform to (7.46) yields the result

$$G_p(x) = \frac{1}{2ja} \sum_{i=-\infty}^{\infty} \left[\frac{e^{j2\pi f x}}{\beta_y} \right]_{f=i/a-k_x/2\pi} \tag{7.47}$$

This summation is an alternative to Equation (7.32) for the direct calculation of the periodic Green's function. Observe that the magnitude of the ith term behaves as

$$0\left(\frac{1}{i}\right) \qquad \text{as } i \to \infty \tag{7.48}$$

Thus, as illustrated in Table 7.1, Equation (7.47) would appear to converge faster than (7.32).

Although preferable to the original summation, Equation (7.47) is not rapidly converging. A more general acceleration procedure can be obtained after introducing a new summation $G_a(x)$ having terms that are asymptotically equal to those of $G_p(x)$ for large i. Then, by combining the Poisson transformation with a decomposition known as *Kummer's transformation* [7], the Green's function can be computed according to

$$G_p(x) = \left[G_p(x) - G_a(x)\right] + F^{-1}\{\tilde{G}_a(f)\} \tag{7.49}$$

where the terms in G_p and G_a cancel for large i. For this procedure to be effective, the Fourier transform of G_a should be a rapidly converging summation.

The transform of $G_p(x)$ is a slowly decaying function as $f \to \infty$ because of the singularity in the Hankel function at $x = 0$. A more rapidly converging function can be obtained by eliminating the singularity. A possible choice for $G_a(x)$ is the function

$$G_a(x) = \frac{1}{4j} \sum_{i=-\infty}^{\infty} H_0^{(2)}\left(k\sqrt{(x-ia)^2+\alpha^2}\right) e^{-jik_x a} \tag{7.50}$$

where the positive parameter α has been introduced in order to eliminate the singularity. (Physically, the addition of this parameter is equivalent to moving the observation point away from the $y = 0$ plane.) The effect of α on the ith term becomes negligible as $i \to \infty$, and G_a and G_p are identical in the asymptotic limit. The Fourier transform of G_a is given by

$$\tilde{G}_a(f) = \frac{1}{2ja} \sum_{i=-\infty}^{\infty} \delta\left(f - \frac{i}{a} + \frac{k_x}{2\pi}\right) \frac{e^{-j\alpha\beta_y}}{\beta_y} \tag{7.51}$$

The inverse Fourier transform produces

$$G_a(x) = \frac{1}{2ja} \sum_{i=-\infty}^{\infty} \left[\frac{e^{j2\pi f x} e^{-j\alpha\beta_y}}{\beta_y} \right]_{f=i/a-k_x/2\pi} \tag{7.52}$$

Since $-j\beta_y$ is a negative real-valued quantity for $(2\pi f)^2 > k^2$, a nonzero α introduces exponential decay into the summation (7.52), making it rapidly convergent. It can also be shown (Prob. P7.7) that for sufficiently large i the ith term of $G_p(x) - G_a(x)$ is proportional to α^2 and is of asymptotic order $O(i^{-3/2})$. Equation (7.49) can be an effective way to compute $G_p(x)$, provided that the parameter α is selected in order to balance the workload required to compute the summation $G_p - G_a$ and the inverse Fourier transform of $\tilde{G}_a$ for a desired accuracy level.

In summary, three ways of computing the periodic Green's function have been considered. The original summation of Equation (7.32) contains terms of $O(i^{-1/2})$ as $i \to \infty$ and

thus is prohibitively slow to converge. The summation obtained from the inverse Fourier transform in (7.47) contains terms of $O(i^{-1})$, while Equations (7.49)–(7.52) involve a summation with terms of $O(i^{-3/2})$. The latter approach offers a substantial improvement on the original summation, as illustrated by a representative example in Table 7.1.

Our ultimate objective is not to evaluate the periodic Green's function, but instead to calculate the matrix entries defined in (7.34). One possibility is to employ numerical quadrature using one of the preceding techniques to obtain G_p at needed values of the integration variable. However, a more efficient approach can be developed that does not require (even as an intermediate step) the computation of the periodic Green's function. Observe that the matrix entries can be written as a convolution,

$$Z_{mn} = jk\eta B(x) * G_p(x)\big|_{x=x_m-x_n} \tag{7.53}$$

where $B(x)$ denotes a pulse basis function defined as

$$B(x) = \begin{cases} 1 & -\frac{1}{2}b < x < \frac{1}{2}b \\ 0 & \text{otherwise} \end{cases} \tag{7.54}$$

Using the convolution theorem

$$B(x) * G_p(x) = F^{-1}\{\tilde{B}(f)\tilde{G}_p(f)\} \tag{7.55}$$

and the Fourier transform

$$\tilde{B}(f) = \frac{\sin(\pi f b)}{\pi f} \tag{7.56}$$

Z_{mn} can be directly obtained in the form of an inverse Fourier transformation,

$$Z_{mn} = \frac{k\eta}{2a}\sum_{i=-\infty}^{\infty}\left[\frac{\sin(\pi f b)}{\pi f}\frac{e^{j2\pi f(x_m-x_n)}}{\beta_y}\right]_{f=i/a-k_x/2\pi} \tag{7.57}$$

The convolution integral in (7.53) is transformed into a multiplication in the Fourier transform domain, and the inverse transform produces a summation for Z_{mn}. Furthermore, the terms appearing in (7.57) behave asymptotically for large i as

$$O\left(\frac{1}{i^2}\right) \tag{7.58}$$

Therefore, by exploiting the convolutional nature of the matrix entries, we eliminate the need to compute G_p directly and at the same time obtain Z_{mn} in the form of a summation that converges faster than the inverse transform summation for the periodic Green's function. Consequently, Equation (7.57) will be a far more efficient alternative than numerical quadrature using the previous expressions for G_p. If other basis and testing functions are employed, with an inner product such as (5.56), analogous formulas may be developed for the general matrix elements

$$Z_{mn} = jk\eta T^{\dagger}(-x) * B(x) * G_p(x)\big|_{x=x_m-x_n} \tag{7.59}$$

The use of smoother testing functions can also help accelerate the convergence of the summation, by contributing additional factors of $1/f$ in the transform domain (Prob. P7.11).

7.5 ALTERNATE ACCELERATION PROCEDURES

The preceding section identified several methods for obtaining the periodic Green's function G_p or the matrix entries Z_{mn}. The most efficient approach of those considered is the summation for Z_{mn} in Equation (7.57), which involves terms of $O(i^{-2})$ as $i \to \infty$.

By combining the convolution of (7.55) with the Poisson and Kummer transformations defined in (7.49), the summation for Z_{mn} may be cast into the slightly more general form [8]

$$\begin{aligned} Z_{mn} = jk\eta \int_{x_n-b/2}^{x_n+b/2} \left[G_p(x_m - x') - G_a(x_m - x')\right] dx' \\ + jk\eta F^{-1}\left\{\frac{\sin(\pi f b)}{\pi f}\tilde{G}_a(f)\right\}_{x=x_m-x_n} \end{aligned} \tag{7.60}$$

where Equation (7.50) can be used for G_a, with the parameter α selected to optimize the computational effort required to evaluate the two terms in (7.60). When $\alpha = 0$, (7.60) reduces to (7.57). When $m = n$, the singularity in the Green's function G_p can be treated by the singularity extraction procedure discussed in Chapter 2 or the generalized Gaussian quadrature algorithm of Appendix A.

In general, (7.60) divides the computational effort between the spatial domain and the Fourier transform (spectral) domain. It is noteworthy that the transform domain summation (the second term) exhibits exponential convergence for $\alpha > 0$. However, the convergence in the spatial domain term $G_p(x) - G_a(x)$ is at best algebraic (Prob. P7.7). Since the spatial domain integral must be evaluated by numerical quadrature, the division of computational effort in (7.60) places a heavy burden on the spatial domain term and a light burden on the spectral domain summation. In fact, the choice $\alpha = 0$ appears optimal [8].

A more balanced division of effort can be obtained by the alternative expression [9]

$$\begin{aligned} Z_{mn} = jk\eta \int_{x_n-b/2}^{x_n+b/2} G_b(x_m - x')\, dx' \\ + jk\eta F^{-1}\left\{\frac{\sin(\pi f b)}{\pi f}\left[\tilde{G}_p(f) - \tilde{G}_b(f)\right]\right\}_{x=x_m-x_n} \end{aligned} \tag{7.61}$$

where

$$G_b(x) = \frac{1}{4j}\sum_{i=-\infty}^{\infty} H_0^{(2)}(-j\gamma\,|x - ia|)e^{-jik_x a} = \frac{1}{2\pi}\sum_{i=-\infty}^{\infty} K_0(\gamma\,|x - ia|)e^{-jik_x a} \tag{7.62}$$

and

$$\tilde{G}_b(f) = \frac{1}{2a}\sum_{i=-\infty}^{\infty} \delta\left(f - \frac{i}{a} + \frac{k_x}{2\pi}\right)\frac{1}{\sqrt{(2\pi f)^2 + \gamma^2}} \tag{7.63}$$

Observe that G_b is obtained by replacing the real-valued wavenumber k in $G_p(x)$ with the imaginary quantity $-j\gamma$. This substitution eliminates the singularity occurring at $(2\pi f)^2 = k^2$ in the Fourier transform $\tilde{G}_p(f)$. Since

$$K_0(u) \approx \sqrt{\frac{\pi}{2u}}e^{-u} \quad \text{as } u \to \infty \tag{7.64}$$

the summation for G_b exhibits exponential convergence. The difference summation in the

second term of (7.61) involves terms that decrease as $O(i^{-4})$ as $i \to \infty$ (Prob. P7.7). Since the integrand necessary for numerical quadrature in (7.61) is exponentially convergent, it should be easier to evaluate than the summation for $G_p(x) - G_a(x)$. Consequently, Equation (7.61) should provide better numerical efficiency than (7.60).

In progressing from the original form of the periodic Green's function in (7.32) to the expression for Z_{mn} in (7.61), the convergence rates of the summations have improved from $O(i^{-1/2})$ to $O(i^{-4})$. However, the convergence of all the preceding expressions is ultimately algebraic. There are alternate approaches that provide exponential convergence, and we turn our attention to two such procedures.

The first approach involves the transformation of G_p into an integral with an exponentially decaying integrand, as suggested by Veysoglu [10]. The development can be based on the geometric series relation

$$\sum_{i=1}^{\infty} e^{-jit} e^{-iu} = \frac{e^{-u} e^{-jt}}{1 - e^{-u} e^{-jt}} \tag{7.65}$$

By multiplying both sides of (7.65) with a function $f(u)$ and integrating, we obtain

$$\sum_{i=1}^{\infty} e^{-jit} \int_0^{\infty} f(u) e^{-iu}\, du = e^{-jt} \int_0^{\infty} \frac{f(u) e^{-u}}{1 - e^{-u} e^{-jt}}\, du \tag{7.66}$$

The integral on the left-hand side of (7.66) can be recognized as the Laplace transform

$$L\{f\} = \tilde{f}(i) = \int_0^{\infty} f(u) e^{-iu}\, du \tag{7.67}$$

which enables us to write the general relation as

$$\sum_{i=1}^{\infty} e^{-jit} L\{f\} = e^{-jt} \int_0^{\infty} \frac{f(u) e^{-u}}{1 - e^{-u} e^{-jt}}\, du \tag{7.68}$$

A Laplace transform pair suitable for use in the present application is [11, 3.364]

$$L\left\{ j \frac{2}{\pi} \frac{1}{\sqrt{u^2 + j2u}} \right\} = e^{ji} H_0^{(2)}(|i|) \tag{7.69}$$

which can be generalized using the scale and shift properties of the Laplace transform to obtain

$$L\left\{ j \frac{2}{\pi} e^{jkx} \frac{e^{-xu/a}}{\sqrt{u^2 + j2kau}} \right\} = e^{jika} H_0^{(2)}(k|x - ia|) \tag{7.70}$$

Substituting (7.70) into (7.68) and assigning the value

$$t = (k + k_x)a \tag{7.71}$$

produce the relation

$$\begin{aligned} &\frac{1}{4j} \sum_{i=1}^{\infty} H_0^{(2)}(k|x - ia|) e^{-jik_x a} \\ &\quad = \frac{K_1 e^{jkx}}{2\pi} \int_0^{\infty} \frac{e^{-(1+x/a)u}}{\sqrt{u^2 + j2kau}(1 - K_1 e^{-u})}\, du \end{aligned} \tag{7.72}$$

where

$$K_1 = e^{-j(k+k_x)a} \tag{7.73}$$

The integrand in (7.72) is singular at $u = 0$, and a change of variables,

$$u = kaw^2 \tag{7.74}$$

can be used to recast (7.72) into the form [10]

$$\begin{aligned}\frac{1}{4j}\sum_{i=1}^{\infty} H_0^{(2)}(k|x-ia|)e^{-jik_x a} \\ = \frac{K_1 e^{jkx}}{\pi}\int_0^{\infty}\frac{e^{-k(a+x)w^2}}{\sqrt{w^2+j2}(1-K_1e^{-kaw^2})}\,dw\end{aligned} \tag{7.75}$$

This summation index in (7.75) runs from 1 to ∞ and therefore is only part of the complete expression for G_p. However, a similar expression can be obtained for negative values of the index and combined with (7.75) to produce

$$\begin{aligned}\frac{1}{4j}\sum_{i=-\infty}^{\infty} H_0^{(2)}(k|x-ia|)e^{-jik_x a} = \frac{1}{4j}H_0^{(2)}(k|x|) \\ +\frac{K_1 e^{jkx}}{\pi}\int_0^{\infty}\frac{e^{-k(a+x)w^2}}{\sqrt{w^2+j2}(1-K_1e^{-kaw^2})}\,dw \\ +\frac{K_2 e^{-jkx}}{\pi}\int_0^{\infty}\frac{e^{-k(a-x)w^2}}{\sqrt{w^2+j2}(1-K_2e^{-kaw^2})}\,dw\end{aligned} \tag{7.76}$$

where

$$K_2 = e^{-j(k-k_x)a} \tag{7.77}$$

In order to obtain the matrix entries Z_{mn} defined in (7.34) for pulse basis functions and delta testing functions, the convolution integral in x can be carried out explicitly to produce

$$\begin{aligned}Z_{mn} = \frac{k\eta}{4}\int_{x_n-\Delta/2}^{x_n+\Delta/2} H_0^{(2)}(k|x_m-x'|)\,dx' \\ +\frac{j2\eta K_1 e^{jk(x_m-x_n)}}{\pi}\int_0^{\infty}\frac{e^{-k(a+x_m-x_n)w^2}\sinh[(j-w^2)k\Delta/2]}{\sqrt{w^2+j2}(j-w^2)(1-K_1e^{-kaw^2})}\,dw \\ +\frac{j2\eta K_2 e^{-jk(x_m-x_n)}}{\pi}\int_0^{\infty}\frac{e^{-k(a-x_m+x_n)w^2}\sinh[(j-w^2)k\Delta/2]}{\sqrt{w^2+j2}(j-w^2)(1-K_2e^{-kaw^2})}\,dw\end{aligned} \tag{7.78}$$

Although the domain of integration in (7.76) and (7.78) extends to infinity, the exponential decay provided by the integrand facilitates an efficient computation by numerical quadrature.

A second approach that provides exponential convergence in the periodic Green's function was developed for the three-dimensional case by Jordan, Richter, and Sheng [12], based on earlier work by Ewald [13]. A two-dimensional adaptation of this idea [14] can be developed using the error function

$$\operatorname{erf}(u) = \frac{2}{\sqrt{\pi}}\int_0^u e^{-t^2}\,dt \tag{7.79}$$

and the complementary error function

$$\operatorname{erfc}(u) = 1 - \operatorname{erf}(u) = \frac{2}{\sqrt{\pi}} \int_u^\infty e^{-t^2}\, dt \tag{7.80}$$

The periodic Green's function can be written as

$$G_p(x) = G_{p1}(x) + G_{p2}(x) \tag{7.81}$$

where

$$G_{p1}(x) = \frac{1}{2a} \sum_{i=-\infty}^{\infty} \left[\operatorname{erfc}\left(\frac{j\beta_y}{E}\right) \frac{e^{j2\pi f x}}{j\beta_y} \right]_{f=i/a-k_x/2\pi} \tag{7.82}$$

$$G_{p2}(x) = \frac{1}{2a} \sum_{i=-\infty}^{\infty} \left[\operatorname{erf}\left(\frac{j\beta_y}{E}\right) \frac{e^{j2\pi f x}}{j\beta_y} \right]_{f=i/a-k_x/2\pi} \tag{7.83}$$

and where β_y is defined in (7.45). The parameter E is arbitrary, to be determined below. Since the complementary error function has the asymptotic behavior

$$\operatorname{erfc}(u) \approx O\left(\frac{e^{-u^2}}{\pi u}\right) \qquad \text{as } u \to \infty \tag{7.84}$$

the summation for G_{p1} exhibits exponential convergence. The summation for G_{p2} in (7.83) contains terms that only decrease as $O(i^{-1})$ as $i \to \infty$ and requires additional manipulation to accelerate the convergence. Using (7.79) and a change of variables, we obtain

$$\begin{aligned} G_{p2}(x) &= \frac{1}{a\sqrt{\pi}} \sum_{i=-\infty}^{\infty} \left[e^{j2\pi f x} \int_0^{1/E} e^{\beta_y^2 s^2}\, ds \right]_{f=i/a-k_x/2\pi} \\ &= \frac{1}{\sqrt{\pi}} \int_0^{1/E} \left(\frac{1}{a} \sum_{i=-\infty}^{\infty} \left[e^{j2\pi f x} e^{\beta_y^2 s^2} \right]_{f=i/a-k_x/2\pi} \right) ds \end{aligned} \tag{7.85}$$

The summation in (7.85) can be recognized as the inverse Fourier transform of a modulated periodic function $\tilde{A}_{mp}(f)$ of the form defined in (7.25), where the generating function is

$$\tilde{A}(f) = e^{\beta_y^2 s^2} = e^{-(2\pi s)^2 f^2} e^{k^2 s^2} \tag{7.86}$$

Consequently, using (7.24) and the inverse Fourier transform

$$A(x) = \frac{1}{2\sqrt{\pi}} \frac{e^{-x^2/(4s^2)} e^{k^2 s^2}}{s} \tag{7.87}$$

the expression in (7.85) can be rewritten as

$$\begin{aligned} G_{p2}(x) &= \frac{1}{2\pi} \int_0^{1/E} \left(\sum_{i=-\infty}^{\infty} \frac{e^{-(x-ia)^2/(4s^2)} e^{k^2 s^2}}{s} e^{-jik_x a} \right) ds \\ &= \frac{1}{2\pi} \sum_{i=-\infty}^{\infty} e^{-jik_x a} \int_0^{1/E} \frac{e^{-(x-ia)^2/(4s^2)} e^{k^2 s^2}}{s}\, ds \end{aligned} \tag{7.88}$$

Finally, after a change of variables

$$u = \frac{1}{4s^2} \tag{7.89}$$

we obtain the spatial domain summation

$$G_{p2}(x) = \frac{1}{4\pi} \sum_{i=-\infty}^{\infty} e^{-jik_x a} \int_{E^2/4}^{\infty} \frac{e^{-(x-ia)^2 u} e^{k^2/(4u)}}{u} du \tag{7.90}$$

The summation in (7.90) exhibits exponential convergence as $i \to \infty$ but is not in a convenient form for computation. The exponential function can be replaced by a Taylor series, converting the integrand in (7.90) according to

$$\frac{e^{-(x-ia)^2 u} e^{k^2/(4u)}}{u} = \sum_{q=0}^{\infty} \left(\frac{k}{2}\right)^{2q} \frac{1}{q!} \frac{e^{-(x-ia)^2 u}}{u^{q+1}} \tag{7.91}$$

The result can be integrated term by term to produce the expression

$$G_{p2}(x) = \frac{1}{4\pi} \sum_{i=-\infty}^{\infty} e^{-jik_x a} \sum_{q=0}^{\infty} \left(\frac{k}{E}\right)^{2q} \frac{1}{q!} E_{q+1}\left\{\tfrac{1}{4}(x - ia)^2 E^2\right\} \tag{7.92}$$

where E_{q+1} is the exponential integral

$$E_{q+1}\{z\} = \int_1^{\infty} \frac{e^{-zt}}{t^{q+1}} dt \tag{7.93}$$

The exponential integral exhibits the asymptotic behavior

$$E_{q+1}\{z\} \approx \frac{e^{-z}}{z} \qquad \text{as } z \to \infty \tag{7.94}$$

and can be evaluated using efficient polynomial approximations [14].

By combining (7.81), (7.82), and (7.92), we obtain an expression for the periodic Green's function in terms of two exponentially convergent summations. In common with the preceding acceleration techniques, the burden has been divided between the spectral domain summation in (7.82) and the spatial domain summation in (7.92). The parameter E determines the balance between these summations, with a large E placing the burden on (7.82) and a small E placing the burden on (7.92). In fact, it can be shown that the choice

$$E > \frac{3\sqrt{d}}{|x|} \tag{7.95}$$

reduces the contribution of $G_{p2}(x)$ to less than 10^{-d} for the range of parameters likely to be of interest [14]. In other words, the entire burden can be shifted to G_{p1} in most cases. Since this is a spectral domain summation, the convolution with the basis function required to compute Z_{mn} can also be incorporated, to produce

$$Z_{mn} \cong \frac{k\eta}{2a} \sum_{i=-\infty}^{\infty} \left[\operatorname{erfc}\left(\frac{j\beta_y}{E}\right) \frac{\sin(\pi f b)}{\pi f} \frac{e^{j2\pi f(x_m - x_n)}}{\beta_y}\right]_{f=i/a-k_x/2\pi} \tag{7.96}$$

for E large enough to satisfy (7.95). The treatment of the case when $x \to 0$ (the diagonal entries Z_{mm}) requires a combination of the spatial and spectral summations [14].

Figure 7.6 illustrates the performance of the exponentially convergent methods suggested in (7.78) and (7.96), compared with the algebraic summation from (7.57), for a representative example. Clearly, for high accuracy the exponentially convergent summations prove far superior to the algebraic methods considered in Section 7.4.

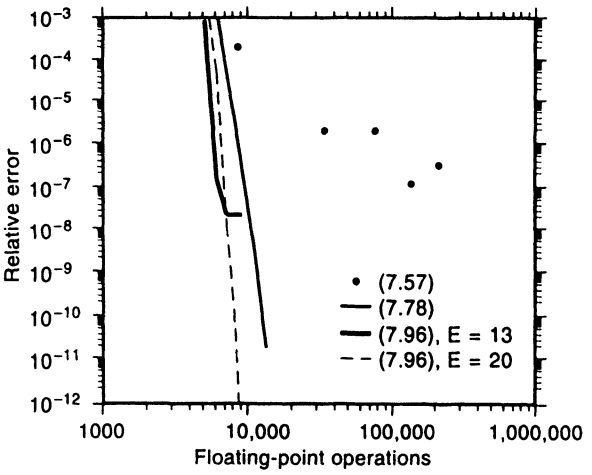

Figure 7.6 Comparison of the required computation (floating-point operations) needed to produce a given accuracy in the matrix entries Z_{mn} for a geometry with $\theta^{inc} = 60°$, $a = 0.8\lambda_0$, $b = 0.05\lambda_0$, and $x_m - x_n = 0.5\lambda_0$.

7.6 BLIND ANGLES

There are values of the period and imposed phase progression for which the periodic Green's function $G_p(x)$ diverges. This can occur if insufficient oscillation is present between successive terms of the summation (7.32); it is more readily observed in the alternative forms of $G_p(x)$ based on inverse Fourier transform summations. [The denominators of Equations (7.47), (7.52), (7.57), and (7.96) vanish if $k^2 = (2\pi f)^2$, while the expression in (7.76) has a singularity if $K_1 = 1$ or $K_2 = 1$.] For a given strip grating, propagation directions of the incident field that result in a divergent $G_p(x)$ are known as the *blind angles* of the strip grating, named after a similar effect in infinite phased-array antennas. Blind angles occur when $(k \pm k_x)a = 2n\pi$ for integer n.

Physically, blind angles arise whenever a Floquet harmonic makes a transition from the invisible to the visible region of the spectrum (from evanescent to propagating character). For example, Figure 7.4 illustrates two harmonics in such a state. Although the periodic Green's function is divergent, the current density remains finite and well behaved at the blind angles (the coefficient of a Floquet harmonic in transition equals zero). Because of a redistribution of the power carried by the various Floquet harmonics at such a transition, irregularities in the reflection and transmission coefficients (*Wood's anomalies*) can be observed as a function of frequency.

For numerical calculations, blind angles can usually be anticipated and avoided. Simple interpolation can be employed in order to determine the behavior of the current density at a blind angle.

7.7 TE SCATTERING FROM A CONDUCTING STRIP GRATING BACKED BY A DIELECTRIC SLAB: EFIE FORMULATION

Generally, strip gratings require a physical support structure that often takes the form of a dielectric slab (Figure 7.7). For analysis purposes, the effect of the slab can be taken

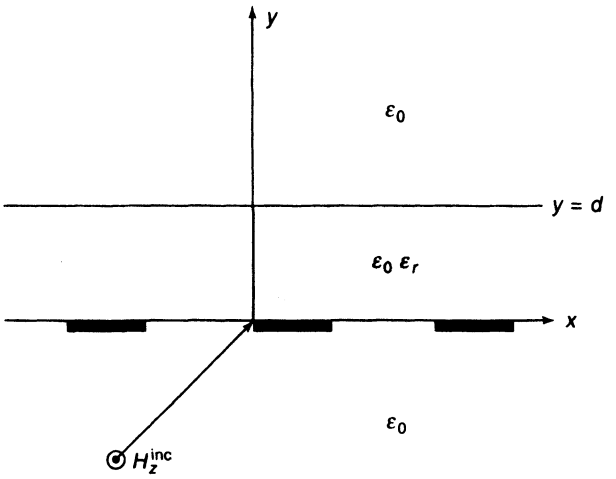

Figure 7.7 Strip grating supported by a dielectric slab illuminated by a TE field.

into account by an appropriate modification of the free-space Green's function. Consider an incident TE plane wave, which only excites the x-component of the current density on the conducting strips. Assuming that the current density explicitly vanishes off of the conductors and that the equation holds only for points on the conducting strips, the EFIE can be written as

$$E_x^{inc}(x,0) = \frac{-1}{j\omega\varepsilon_0}\left(\frac{\partial^2}{\partial x^2} + k^2\right)\int_{-\infty}^{\infty} J_x(x')G_d(x-x')\,dx' \tag{7.97}$$

where G_d represents the Green's function for an individual line source of x-directed electric current radiating on the surface of a dielectric slab (Figure 7.8). In order to derive the Green's function, we observe that the line source can be expressed as an inverse Fourier transform

$$J_x(x,y) = \delta(x)\delta(y) = \delta(y)\int_{-\infty}^{\infty} e^{j2\pi fx}\,df \tag{7.98}$$

which can be thought of as the superposition of current sheets of the form

$$J_x(x) = e^{j2\pi fx} \tag{7.99}$$

The response of each current sheet can be obtained by the solution of a one-dimensional wave equation or, equivalently, through the use of a transmission line analogy as illustrated in Figure 7.9. The parameters employed in the transmission line analogy are the TE-wave impedances

$$Z_0 = -\frac{E_x}{H_z} = \frac{\eta k_y}{k} \tag{7.100}$$

$$Z_d = \frac{\eta_d k_{dy}}{k_d} \tag{7.101}$$

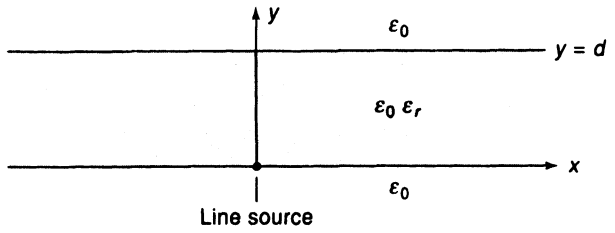

Figure 7.8 Line source radiating on the surface of a dielectric slab.

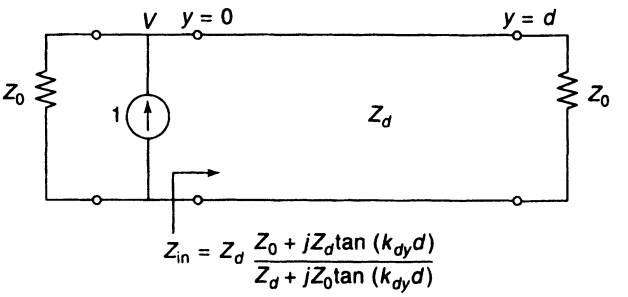

Figure 7.9 Equivalent transmission line model for a line source radiating on the surface of a dielectric slab.

$$V = \frac{Z_0 Z_{in}}{Z_0 + Z_{in}} = \frac{Z_d\left(1 + j\frac{Z_d}{Z_0}\tan[k_{dy}d]\right)}{2\frac{Z_d}{Z_0} + j\left(1 + \left[\frac{Z_d}{Z_0}\right]^2\right)\tan[k_{dy}d]}$$

where η and η_d represent the intrinsic impedance of the background medium and the dielectric slab, respectively, and k and k_d denote the wavenumber of the background medium and the dielectric slab, respectively,

$$k_y = \sqrt{k^2 - (2\pi f)^2} \tag{7.102}$$

and

$$k_{dy} = \sqrt{k_d^2 - (2\pi f)^2} \tag{7.103}$$

After solving the transmission line circuit of Figure 7.9, we obtain the electric field due to a single current sheet, which has the form

$$E_x^{\text{sheet}}(x, 0) = \frac{-k_{dy}}{2\omega\varepsilon_d} \frac{1 + j(k_{dy}/\varepsilon_r k_y)\tan(k_{dy}d)}{k_{dy}/\varepsilon_r k_y + j(1/2)\left[1 + \left(k_{dy}/\varepsilon_r k_y\right)^2\right]\tan(k_{dy}d)} e^{j2\pi f x} \tag{7.104}$$

The electric field due to a unit line source is the superposition of the fields produced by the current sheets, which can be expressed as

$$E_x(x, 0) = \int_{-\infty}^{\infty} E_x^{\text{sheet}}(x, 0)\, df \tag{7.105}$$

Since the electric field due to the line source can also be found from

$$E_x(x, 0) = \frac{1}{j\omega\varepsilon_0}\left(\frac{\partial^2}{\partial x^2} + k^2\right) G_d(x) \tag{7.106}$$

we obtain the Green's function G_d as

$$G_d(x) = \int_{-\infty}^{\infty} \frac{1}{2j\varepsilon_r k_{dy}} \frac{1 + j(k_{dy}/\varepsilon_r k_y)\tan(k_{dy}d)}{k_{dy}/\varepsilon_r k_y + j(1/2)\left[1 + \left(k_{dy}/\varepsilon_r k_y\right)^2\right]\tan(k_{dy}d)} e^{j2\pi f x}\, df \tag{7.107}$$

Because of the integral, this Green's function is cumbersome for direct evaluation. However, the Fourier transform is the algebraic expression

$$\tilde{G}_d(f) = \frac{1}{2j\varepsilon_r k_{dy}} \frac{1 + j(k_{dy}/\varepsilon_r k_y)\tan(k_{dy}d)}{k_{dy}/\varepsilon_r k_y + j(1/2)\left[1 + \left(k_{dy}/\varepsilon_r k_y\right)^2\right]\tan(k_{dy}d)} \tag{7.108}$$

Consequently, we seek a formulation where the Green's function need only be evaluated in the Fourier transform domain.

For a strip grating illuminated by a TE incident plane wave, the current density satisfies the Floquet condition

$$J_x(x+a) = J_x(x)e^{-jk_x a} \tag{7.109}$$

Therefore, the EFIE of (7.97) can be expressed as an integral over a single period of the structure, namely,

$$E_x^{\text{inc}}(x,0) = -\frac{1}{j\omega\varepsilon_0}\left(\frac{\partial^2}{\partial x^2}+k^2\right)\int_{\text{single strip}} J_x(x')G_{dp}(x-x')\,dx' \tag{7.110}$$

where we now employ the periodic Green's function

$$G_{dp}(x) = \sum_{i=-\infty}^{\infty} G_d(x-ia)e^{-jik_x a} \tag{7.111}$$

To effect a solution, we divide the strip into equal-sized cells and introduce basis and testing functions in order to approximate the current density by

$$J_x(x) \cong \sum_{n=1}^{N} j_n B(x-x_n) \tag{7.112}$$

and discretize the EFIE into the matrix equation

$$\int T^{\dagger}(x-x_m)E_x^{\text{inc}}(x,0)\,dx = \sum_{n=1}^{N} j_n Z_{mn} \qquad m = 1,2,\ldots,N \tag{7.113}$$

where

$$Z_{mn} = -\frac{1}{j\omega\varepsilon_0}\left(\frac{\partial^2}{\partial x^2}+k^2\right)\int T^{\dagger}(x-x_m)\int B(x'-x_n)G_{dp}(x-x')\,dx'\,dx \tag{7.114}$$

and appropriate limits of integration are implied. Following the approach outlined in Section 7.4, the matrix entries can be expressed in general form as the inverse Fourier transformation

$$\begin{aligned} Z_{mn} &= -\frac{1}{j\omega\varepsilon_0}\left(\frac{\partial^2}{\partial x^2}+k^2\right)T^R(x) * B(x) * G_{dp}(x)|_{x=x_m-x_n} \\ &= F^{-1}\left\{\frac{(2\pi f)^2-k^2}{j\omega\varepsilon_0}\tilde{T}^R(f)\tilde{B}(f)\tilde{G}_{dp}(f)\right\}_{x=x_m-x_n} \\ &= \sum_{i=-\infty}^{\infty}\left[\frac{(2\pi f)^2-k^2}{j\omega\varepsilon_0 a}e^{j2\pi f(x_m-x_n)}\tilde{T}^R(f)\tilde{B}(f)\tilde{G}_d(f)\right]_{f=i/a-k_x/2\pi} \end{aligned} \tag{7.115}$$

where $T^R(x) = T^{\dagger}(-x)$.

In Chapter 2, subsectional triangle basis functions and pulse testing functions were employed to discretize the EFIE for TE scattering from a single strip or cylinder. It is reasonable to suppose that these same functions will provide a robust discretization for this TE strip grating example. The Fourier transforms of a triangle and pulse function (Figure 2.8) are

$$F\{t(x;-b,0,b)\} = \tilde{B}(f) = \frac{\sin^2(\pi bf)}{b(\pi f)^2} \tag{7.116}$$

and

$$F\left\{p\left(x;-\frac{1}{2}b,\frac{1}{2}b\right)\right\}=\tilde{T}^R(f)=\frac{\sin(\pi bf)}{\pi f} \tag{7.117}$$

We observe from these equations and (7.108) that for large values of the index i, the magnitude of the ith term in (7.115) behaves as

$$O\left(\frac{1}{i^2}\right) \tag{7.118}$$

Therefore, the use of these basis and testing functions will provide enough decay as $i \to \infty$ to ensure convergence of the summation. If desired, a faster scheme for the computation of the matrix elements may be developed based on the ideas discussed in Section 7.5.

7.8 APERTURE FORMULATION FOR TM SCATTERING FROM A CONDUCTING STRIP GRATING

Previous sections have considered formulations where the primary unknown is the equivalent electric surface current located on perfectly conducting material. For periodic geometries with large conducting regions and small apertures between them, it may be more efficient to treat the tangential electric field in the aperture (or the equivalent magnetic surface current in the aperture) as the primary unknown. Consider the case of TM scattering from a conducting grating such as illustrated in Figure 7.3. Based on the aperture formulation discussed in Section 1.10, we can write an integral equation for the strip grating problem as

$$H_x^{\text{inc}}(x,0)=-\frac{2}{j\omega\mu_0}\left(\frac{\partial^2}{\partial x^2}+k^2\right)\int_{\text{single aperture}} K_x(x')G_p(x-x')\,dx' \tag{7.119}$$

where G_p is the periodic Green's function defined in (7.32) and K_x is the equivalent magnetic current in the aperture, defined so that $K_x(x)=E_z(x,0)$. The incident magnetic field is that field produced by the original source in the absence of the grating.

The method-of-moments discretization of (7.119) follows in the usual manner and produces a matrix equation $\mathbf{Zk}=\mathbf{h}$, where the general form for the entries is given by

$$\begin{aligned} Z_{mn}&=-\frac{2}{j\omega\mu_0}\left(\frac{\partial^2}{\partial x^2}+k^2\right)T^R(x)*B(x)*G_p(x)|_{x=x_m-x_n}\\ &=-2F^{-1}\left\{\frac{k^2-(2\pi f)^2}{j\omega\mu_0}\tilde{T}^R(f)\tilde{B}(f)\tilde{G}_p(f)\right\}_{x=x_m-x_n}\end{aligned} \tag{7.120}$$

and

$$h_m=\int_{\text{aperture}} T(x_m-x)H_x^{\text{inc}}(x)\,dx \tag{7.121}$$

where $T^R(x)=T^\dagger(-x)$. As in the preceding section, it is reasonable to suppose that subsectional triangle basis functions and pulse testing functions are sufficient to discretize the integral operator. The acceleration procedures discussed in Sections 7.4 and 7.5 can be incorporated as needed.

After the coefficients of the magnetic current density in the apertures have been determined, the scattered field can be expressed in terms of the Floquet harmonics. The approach is the electromagnetic dual to that considered in Prob. P7.6 for the TE polarization.

7.9 SCATTERING MATRIX ANALYSIS OF CASCADED PERIODIC SURFACES [4, 15, 16]

Because strip gratings allow complete transmission at certain frequencies and complete reflection at other frequencies, they are a simple type of *frequency-selective surface*. A wide variety of filter characteristics can be obtained by cascading multiple layers of frequency-selective surfaces. To efficiently analyze multilayered structures, each periodic surface can be modeled as a multiport network with each port representing one Floquet harmonic of a given polarization. The coefficients of each propagating Floquet harmonic determine the "far-field" reflection and transmission characteristics of periodic surfaces. A complete near-zone model will generally require a combination of propagating and evanescent harmonics. Generalized scattering and transmission matrices representing each individual surface can subsequently be employed as a building block in the electromagnetic model of a multilayered structure.

The definition of a scattering matrix is presented in the context of a two-port network in Figure 7.10. For TM excitation, the scattering matrix arising from the strip grating problem is a 2-by-2 block matrix of the form

$$\mathbf{S} = \begin{bmatrix} S_{11} & S_{12} \\ S_{21} & S_{22} \end{bmatrix} \tag{7.122}$$

where each of the blocks comprising (7.122) are infinite-dimensional matrices relating the coefficients of the scattered Floquet harmonics to those of the incident harmonics. These blocks take the form

$$S_{11} = \begin{bmatrix} s_{11}^{11} & s_{12}^{11} & \cdots \\ s_{21}^{11} & s_{22}^{11} & \\ s_{31}^{11} & s_{32}^{11} & \\ \vdots & & \end{bmatrix} \tag{7.123}$$

In practice, these matrices are truncated to finite dimension. The entries of the generalized

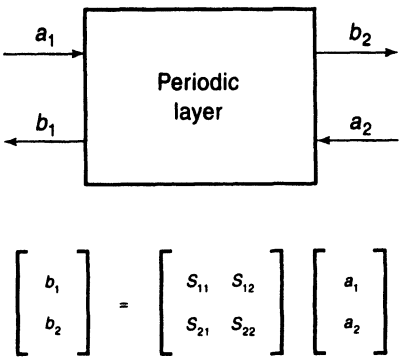

Figure 7.10 Two-port scattering parameters.

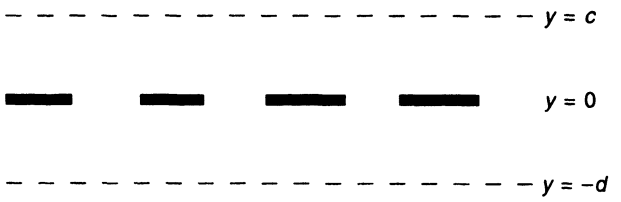

Figure 7.11 Location of reference planes for the definition of S-parameters.

scattering matrices depend on the location of reference planes as indicated in Figure 7.11.

There are a variety of ways to define the scattering parameters, and we use the definitions employed in microwave circuit analysis [17]. The (m, n) entry in the scattering matrix of Equation (7.122) is proportional to the square root of the ratio of the power carried by the mth reflected harmonic to the power carried by the nth incident harmonic. In general, this is a complex-valued quantity having magnitude

$$\text{mag}(s_{mn}^{11}) = \sqrt{\frac{\displaystyle\int_0^a \left|\bar{E}_m^s \times \bar{H}_m^{s\dagger} \cdot \hat{y}\right|_{y=-d} dx}{\displaystyle\int_0^a \left|\bar{E}_n^{\text{inc}} \times \bar{H}_n^{\text{inc}\dagger} \cdot \hat{y}\right|_{y=-d} dx}} \tag{7.124}$$

and phase equal to the difference of the phase of the corresponding electric field harmonic at the output and input reference planes, that is,

$$\text{phase}(s_{mn}^{11}) = \text{phase}\{E_{zm}^s(0, -d)\} - \text{phase}\{E_{zn}^{\text{inc}}(0, -d)\} \tag{7.125}$$

Using the form of the Floquet harmonics specified in Equation (7.22), the magnitude of the (m, n) entry can be simplified to

$$\text{mag}(s_{mn}^{11}) = \frac{|e_m|}{|e_n^{\text{inc}}|}\sqrt{\left|\frac{\sqrt{k^2 - k_{xm}^2}}{\sqrt{k^2 - k_{xn}^2}}\right|} \tag{7.126}$$

The entries of the S_{21} matrix are defined in a similar manner, only in terms of the total transmitted fields instead of the scattered reflected fields. In other words,

$$\text{mag}(s_{mn}^{21}) = \sqrt{\frac{\displaystyle\int_0^a \left|\bar{E}_m^{\text{tot}} \times \bar{H}_m^{\text{tot}\dagger} \cdot \hat{y}\right|_{y=c} dx}{\displaystyle\int_0^a \left|\bar{E}_n^{\text{inc}} \times \bar{H}_n^{\text{inc}\dagger} \cdot \hat{y}\right|_{y=-d} dx}} \tag{7.127}$$

and

$$\text{phase}(s_{mn}^{21}) = \text{phase}\{E_{zm}^{\text{tot}}(0, c)\} - \text{phase}\{E_{zn}^{\text{inc}}(0, -d)\} \tag{7.128}$$

The S_{12} and S_{22} matrices are defined in an analogous manner.

For a single surface illuminated by a plane wave, generalized reflection and transmission coefficients are sometimes employed as an alternative to the scattering matrix description. The magnitudes of these expressions simplify to

$$|R_n| = \text{mag}(s_{n0}^{11}) = \frac{|e_n|}{|E_0|}\sqrt{\left|\frac{\sqrt{k^2 - k_{xn}^2}}{\sqrt{k^2 - k_x^2}}\right|} \tag{7.129}$$

and

$$|T_n| = \text{mag}(s_{n0}^{21}) = \left| \delta_0^n + \frac{e_n}{E_0} \sqrt{\left| \frac{\sqrt{k^2 - k_{xn}^2}}{\sqrt{k^2 - k_x^2}} \right|} \right| \tag{7.130}$$

and the phases are defined in accordance with Equations (7.125) and (7.128).

For cascading several layers, the transmission matrix representation

$$\begin{bmatrix} b_2 \\ a_2 \end{bmatrix} = \begin{bmatrix} T_{11} & T_{12} \\ T_{21} & T_{22} \end{bmatrix} \begin{bmatrix} a_1 \\ b_1 \end{bmatrix} \tag{7.131}$$

(see Figure 7.10 for a definition of the a's and b's) is more convenient than the scattering matrix description, and can be found from the elements of the scattering matrix according to

$$T_{11} = S_{21} - S_{22} S_{12}^{-1} S_{11} \tag{7.132}$$

$$T_{12} = S_{22} S_{12}^{-1} \tag{7.133}$$

$$T_{21} = -S_{12}^{-1} S_{11} \tag{7.134}$$

$$T_{22} = S_{12}^{-1} \tag{7.135}$$

As an example, suppose we cascade three gratings represented by transmission matrices T_1, T_2, and T_3, where the excitation passes through grating 1 before gratings 2 and 3. The composite transmission matrix is given by

$$T = T_3 T_2 T_1 \tag{7.136}$$

Of course, the cascading process requires that a common set of Floquet harmonics be employed within the scattering or transmission matrix description of each grating.

The process of cascading may become numerically unstable if higher order (evanescent) harmonics are cascaded over large distances. As a consequence of the exponential decay these terms experience, the transmission matrices may become extremely ill-conditioned as the terminal planes are separated [4]. Under these conditions, it may be advantageous to construct composite scattering matrices by an alternative process discussed in the literature [4, 18, 19].

7.10 TM SCATTERING FROM A HALF-SPACE HAVING A GENERAL PERIODIC SURFACE: EFIE DISCRETIZED WITH PULSE BASIS FUNCTIONS AND DELTA TESTING FUNCTIONS [20]

Figure 7.12 depicts two regions separated by an interface whose location in y varies periodically with x. We desire to determine the reflected and transmitted fields in response to a TM plane wave

$$E_z^{\text{inc}}(x, y) = E_0 e^{-jk_1(x\cos\theta + y\sin\theta)} \tag{7.137}$$

incident from the lower region. Huygens' equivalence principle can be used to develop an equivalent model of each region in terms of electric and magnetic sources $J_z(t)$ and $K_t(t)$ on

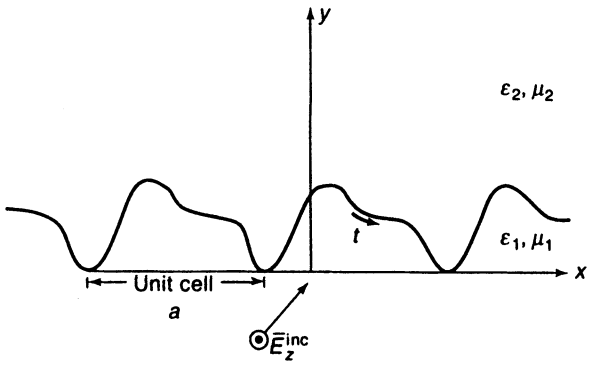

Figure 7.12 Periodic interface between two semi-infinite regions. A TM wave is incident from region 1.

the surface, where t is a parametric variable defined in Figure 7.12. Following the general procedure discussed in Section 1.9, coupled EFIEs can be constructed of the form

$$E_z^{\text{inc}}(t) = K_t(t) + jk_1\eta_1 A_z^1(t) + \hat{z} \cdot \nabla \times \bar{F}_t^1|_{S^+} \tag{7.138}$$

$$0 = -K_t(t) + jk_2\eta_2 A_z^2(t) + \hat{z} \cdot \nabla \times \bar{F}_t^2|_{S^-} \tag{7.139}$$

where

$$A_z^i(t) = \int_{-\infty}^{\infty} J_z(t') \frac{1}{4j} H_0^{(2)}(k_i R)\, dt' \tag{7.140}$$

$$\bar{F}_t^i(t) = \int_{-\infty}^{\infty} \hat{t}(t') K_t(t') \frac{1}{4j} H_0^{(2)}(k_i R)\, dt' \tag{7.141}$$

and

$$R = \sqrt{[x(t) - x(t')]^2 + [y(t) - y(t')]^2} \tag{7.142}$$

The superscript on A_z and F_t denotes the medium. For generality, region 2 may be lossy. Equation (7.138) is enforced an infinitesimal distance outside (i.e., the region 1 side) of the interface, while (7.139) is enforced an infinitesimal distance inside the interface.

The plane-wave excitation imposes a progressive phase shift with phase constant

$$k_x = k_1 \cos\theta \tag{7.143}$$

and the equivalent currents must satisfy the Floquet conditions

$$J_z(x + a, y) = J_z(x, y) e^{-jk_x a} \tag{7.144}$$

$$K_t(x + a, y) = K_t(x, y) e^{-jk_x a} \tag{7.145}$$

As a consequence of these relationships, the domain of the integral operators can be transformed to a single period so that

$$A_z^i(t) = \int_{\text{one period}} J_z(t') G_p^i(x(t) - x(t'), y(t) - y(t'))\, dt' \tag{7.146}$$

$$\bar{F}_t^i(t) = \int_{\text{one period}} \hat{t}(t') K_t(t') G_p^i(x(t) - x(t'), y(t) - y(t'))\, dt' \tag{7.147}$$

where the periodic Green's function is given by

$$G_p^i(x, y) = \frac{1}{4j} \sum_{q=-\infty}^{\infty} H_0^{(2)} \left[k_i \sqrt{(x - qa)^2 + y^2} \right] e^{-jqk_x a} \tag{7.148}$$

Numerical solutions can be obtained in the context of the method of moments. Suppose that one period of the surface is divided into N cells, as depicted in Figure 7.13. The equivalent currents can be represented by the expansions

$$J_z(t) \cong \sum_{n=1}^{N} j_n B_n(t) \tag{7.149}$$

$$K_t(t) \cong \sum_{n=1}^{N} h_n B_n(t) \tag{7.150}$$

where B_n denotes a pulse basis function having constant support over cell n. The coupled equations can be enforced at the centers of each interval (Dirac delta testing functions) to produce a matrix equation

$$\begin{bmatrix} \mathbf{A} & \mathbf{B} \\ \mathbf{C} & \mathbf{D} \end{bmatrix} \begin{bmatrix} j_1 \\ j_2 \\ \cdot \\ \cdot \\ \cdot \\ j_N \\ h_1 \\ h_2 \\ \cdot \\ \cdot \\ \cdot \\ h_N \end{bmatrix} = \begin{bmatrix} e_1 \\ e_2 \\ \cdot \\ \cdot \\ \cdot \\ e_N \\ 0 \\ 0 \\ \cdot \\ \cdot \\ \cdot \\ 0 \end{bmatrix} \tag{7.151}$$

where

$$A_{mn} = jk_1\eta_1 \int_{\text{cell } n} G_p^1(x(t_m) - x(t'), y(t_m) - y(t'))\, dt' \tag{7.152}$$

$$B_{mn} = -\int_{\text{cell } n} \hat{z} \cdot \hat{t}_n \times \nabla G_p^1|_{x(t_m)-x(t'),y(t_m)-y(t')}\, dt' \qquad m \neq n \tag{7.153}$$

$$B_{mm} \cong \frac{1}{2} - \int_{\text{cell } m} \hat{z} \cdot \hat{t}_n \times \nabla G_p^{1m}\, dt' \tag{7.154}$$

$$C_{mn} = jk_2\eta_2 \int_{\text{cell } n} G_p^2\, dt' \tag{7.155}$$

$$D_{mn} = -\int_{\text{cell } n} \hat{z} \cdot \hat{t}_n \times \nabla G_p^2\, dt' \qquad m \neq n \tag{7.156}$$

$$D_{mm} \cong -\frac{1}{2} - \int_{\text{cell } m} \hat{z} \cdot \hat{t}_n \times \nabla G_p^{2m}\, dt' \tag{7.157}$$

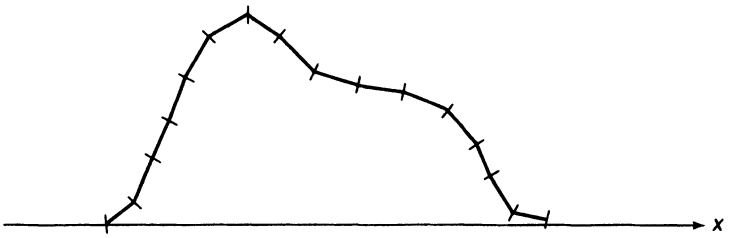

Figure 7.13 Flat-cell model of one period of the surface in Figure 7.12.

and

$$e_m = E_0 e^{-jk_1[x(t_m)\cos\theta + y(t_m)\sin\theta]} \tag{7.158}$$

In the preceding equations, t_n represents the center of cell n, and G_p^{im} denotes G_p^i with the $q = 0$ term omitted from the summation of Equation (7.148). The arguments of each integrand are the same as those in (7.152) and (7.153). Equations (7.154) and (7.157) represent the situation in which the source and observation cells coincide; these expressions were obtained by a limiting procedure that is exact if the cells are flat and a good approximation if the cells have a large radius of curvature (see Chapter 2).

Because the periodic Green's function of (7.148) is a slowly converging summation, the efficient evaluation of the matrix entries requires some sort of acceleration procedure. Consider the evaluation of A_{mn}. In Section 7.4, a similar summation was accelerated using the convolution theorem. Although the matrix entry in (7.152) is also a convolution between the pulse basis function and the Green's function, the domain of the pulse function is not necessarily located parallel to the x-axis in this case. For a general orientation, the basis function will be a Dirac delta function in x. Since the Fourier transform of a delta function is constant, the convolution will not provide a means of accelerating the summation.

The Fourier transform of the periodic Green's function has the form

$$\tilde{G}_p^i(f, y) = \frac{1}{2ja} \sum_{q=-\infty}^{\infty} \delta\left(f - \frac{q}{a} + \frac{k_x}{2\pi}\right) \frac{e^{-j\beta_{yi}|y|}}{\beta_{yi}} \tag{7.159}$$

where, for the lossless region 1,

$$\beta_{y1} = \begin{cases} \sqrt{k_1^2 - (2\pi f)^2} & k_1^2 > (2\pi f)^2 \\ -j\sqrt{(2\pi f)^2 - k_1^2} & k_1^2 < (2\pi f)^2 \end{cases} \tag{7.160}$$

Note that the function in (7.159) exhibits exponential decay as $f \to \infty$ for nonzero y, suggesting in that case that the periodic Green's function can be directly evaluated in terms of the inverse Fourier transform summation. However, a more general acceleration procedure is required if the separation in y vanishes or becomes very small, since the inverse Fourier transform summation might then be slow to converge. Any of the acceleration procedures from Sections 7.4 and 7.5 can be adapted to (7.152)–(7.157). One approach has been developed using algebraic acceleration, and the reader is referred to [20] for detailed expressions for the matrix entries. It is likely that a more computationally efficient scheme could be contrived using one of the exponential acceleration techniques (Section 7.5).

The TM-to-z formulation can be adapted to the TE polarization using the ideas of electromagnetic duality and can be obtained from the preceding expressions by exchanging

the electric and magnetic fields, currents, and medium parameters according to the duality relationships presented in Section 1.5.

We will illustrate the accuracy of the procedure for the TE case. Figure 7.14 depicts a corrugated surface separating a region of free space from a region with relative permittivity $\varepsilon_r = 2.5$ and relative permeability $\mu_r = 1$. The triangular corrugation has a period equal to 1.0 λ, where λ denotes the free-space wavelength. A uniform plane wave is incident upon the interface at an angle 30° from normal. Figure 7.15 compares the magnitudes of the Floquet harmonics as a function of the corrugation depth, as produced by this approach (as implemented in reference [20]) and a "coupled-wave" formulation described in reference [21]. Good agreement is observed between the two formulations, neither of which is exact. The accuracy of the integral equation approach is primarily limited by the finite number of basis functions; the approach of reference [21] is primarily limited by the finite number of Floquet harmonics used within a field expansion throughout the corrugated region. For the data shown in Figure 7.15, a density of approximately 20 cells/λ was used within the integral equation approach and a total of nine Floquet harmonics were used with the approach of reference [21].

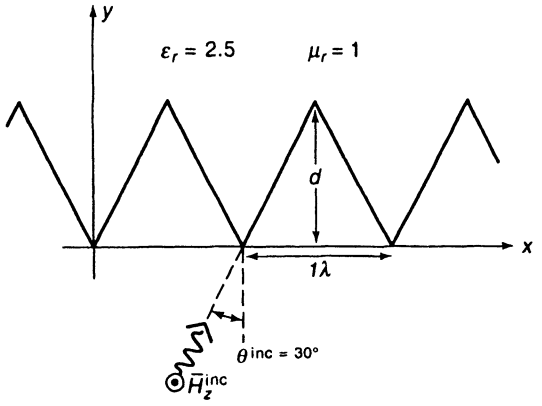

Figure 7.14 Triangular corrugated interface between two regions. Region 1 is free space, region 2 has $\epsilon_r = 2.5$. A TE wave is incident from region 1.

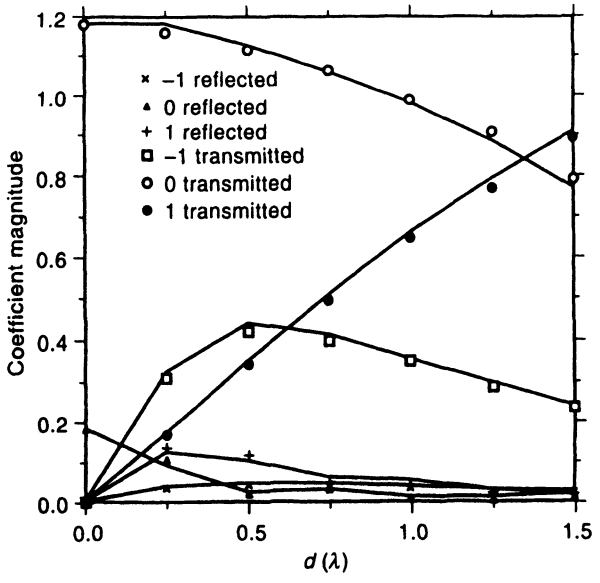

Figure 7.15 Comparison of Floquet coefficients produced by the integral equation formulation (solid line) and the coupled-mode formulation of reference [21] (markers) applied to the geometry depicted in Figure 7.14. After [20].

Although the preceding discussion was confined to a continuous periodic surface, Equations (7.152)–(7.154) also provide the exterior matrix entries necessary to treat an array of individual two-dimensional homogeneous dielectric scatterers exhibiting one-dimensional periodicity. The above approach is easily adapted to the discrete situation by incorporating analogous integral expressions for the interior interactions, which do not require a periodic Green's function (Prob. P7.17).

7.11 TM SCATTERING FROM AN INHOMOGENEOUS GRATING: OUTWARD-LOOKING FORMULATION WITH AN INTEGRAL EQUATION RBC [22]

To treat highly heterogeneous geometries, such as the periodic structure illustrated in Figure 7.16, the integral formulations described in this chapter could be extended to volume equations. However, every matrix entry arising within a surface or volume integral formulation for periodic geometries involves a time-consuming summation over the periodic Green's function. As an alternative approach for heterogeneous structures, we turn our attention to an outward-looking differential equation formulation similar to those introduced in Chapter 3. In a differential equation formulation, the periodicity is incorporated through boundary conditions. Consequently, the matrix entries associated with interior interactions are identical to those of a general nonperiodic structure (Chapter 3). Furthermore, because the shape of the unit cell is arbitrary, it is convenient to employ planar radiation boundaries along the direction of periodicity. Planar boundaries simplify the calculations associated with an RBC, since the convolution idea described in Section 7.4 can be used to accelerate the periodic Green's function summation within the RBC.

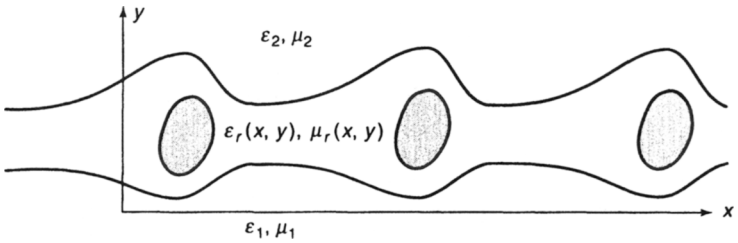

Figure 7.16 Inhomogeneous structure with periodicity along the x direction.

Suppose that the periodic structure of Figure 7.16 is illuminated by a TM-to-z wave incident from the lower ($y < 0$) region. The computational domain may be truncated at the unit cell depicted in Figure 7.17. The interior region Γ associated with a single unit cell is bounded by flat surfaces $\partial\Gamma_1$ and $\partial\Gamma_2$ parallel to the x-axis and arbitrarily shaped surfaces $\partial\Gamma_3$ and $\partial\Gamma_4$. These boundaries are translations of a common surface along the direction of periodicity, so that a TM incident wave

$$E_z^{\text{inc}}(x, y) = E_0 e^{-jk_1(x\cos\theta + y\sin\theta)} \tag{7.161}$$

imposes a Floquet condition

$$E_z(x, y)\,|_{\partial\Gamma_4} = E_z(x, y)\,|_{\partial\Gamma_3}\, e^{-jk_x a} \tag{7.162}$$

where $k_x = k_1 \cos\theta$, constraining the fields on $\partial\Gamma_3$ and $\partial\Gamma_4$.

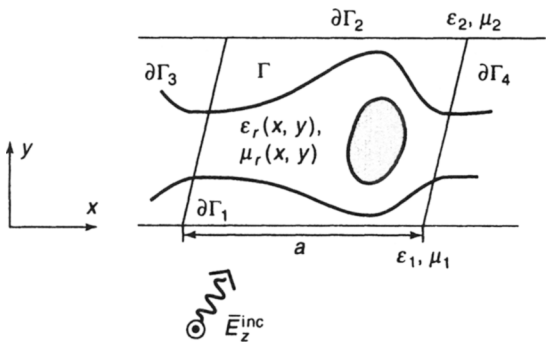

Figure 7.17 Unit cell defined by boundaries $\partial\Gamma_1$ and $\partial\Gamma_2$ parallel to the x-axis and boundaries $\partial\Gamma_3$ and $\partial\Gamma_4$ on which a Floquet condition must hold.

The fields throughout the interior region Γ must satisfy the scalar Helmholtz equation, which can be written in weak form as

$$\iint_\Gamma \frac{1}{\mu_r}\nabla T \cdot \nabla E_z - k^2 \varepsilon_r T E_z = \int_{\partial\Gamma_1+\partial\Gamma_2+\partial\Gamma_3+\partial\Gamma_4+\partial\Gamma_c} \frac{1}{\mu_r} T \frac{\partial E_z}{\partial n} \tag{7.163}$$

where $\partial\Gamma_c$ denotes the boundaries of any imbedded perfectly conducting regions, if present. The integral over $\partial\Gamma_c$ vanishes, as previously explained in Chapter 3. The integrals over boundaries $\partial\Gamma_3$ and $\partial\Gamma_4$ also vanish, provided that the periodicity is explicitly incorporated into the global finite-element system during the matrix construction phase of the analysis. We illustrate this process below. The boundary integrals over $\partial\Gamma_1$ and $\partial\Gamma_2$ provide a means for coupling the incident field to the Helmholtz equation and also for imposing an RBC. Specifically, we consider an RBC obtained from the EFIE.

Assuming the existence of a normal vector $\hat{n}$ pointing out of the region Γ and a tangent vector $\hat{t}$ defined so that $\hat{n} \times \hat{t} = \hat{z}$, equivalent sources can be introduced on $\partial\Gamma_1$ and $\partial\Gamma_2$ according to

$$J_z = \hat{z} \cdot \hat{n} \times \bar{H} = H_t = \frac{1}{jk\eta}\frac{\partial E_z}{\partial n} \tag{7.164}$$

$$K_t = \hat{t} \cdot \bar{E} \times \hat{n} = E_z \tag{7.165}$$

where k and η are the wavenumber and intrinsic impedance, respectively, of the medium along each boundary. Therefore, the boundary integrals over $\partial\Gamma_1$ and $\partial\Gamma_2$ can be replaced by

$$j\omega\mu_0 \int_{\partial\Gamma_1} T(t) J_z(t)\, dt \quad \text{and} \quad j\omega\mu_0 \int_{\partial\Gamma_2} T(t) J_z(t)\, dt \tag{7.166}$$

Suppose that the computational domain Γ is divided into triangular cells, over which the field is represented by a piecewise-linear basis (the "pyramid" functions of Chapter 3)

$$E_z(x, y) \cong \sum_{n=1}^{N} e_n B_n(x, y) \tag{7.167}$$

In addition, let the electric current density $J_z(t)$ along boundaries $\partial\Gamma_1$ and $\partial\Gamma_2$ be replaced by the piecewise-linear (subsectional triangle) expansion

$$J_z(t) \cong \sum_{n=1}^{M} j_n B_n(t) \tag{7.168}$$

For convenience, we choose testing functions $T_m(x, y) = B_m(x, y)$ and discretize Equation (7.163) into matrix form to obtain

$$\begin{bmatrix} \mathbf{I} & \mathbf{I}_1^T & \mathbf{I}_2^T & \mathbf{0} & \mathbf{0} \\ \mathbf{I}_1 & \mathbf{E}_1 & \mathbf{0} & \mathbf{J}_1 & \mathbf{0} \\ \mathbf{I}_2 & \mathbf{0} & \mathbf{E}_2 & \mathbf{0} & \mathbf{J}_2 \end{bmatrix} \begin{bmatrix} \mathbf{e}^{\text{int}} \\ \mathbf{e}_1 \\ \mathbf{e}_2 \\ \mathbf{j}_1 \\ \mathbf{j}_2 \end{bmatrix} = \begin{bmatrix} \mathbf{0} \\ \mathbf{0} \\ \mathbf{0} \end{bmatrix} \tag{7.169}$$

where the submatrix $\mathbf{I}$ contains all of the interactions between basis and testing functions centered at interior nodes of the mesh, submatrices $\mathbf{I}_1$ and $\mathbf{I}_2$ contain all of the interactions between interior basis functions and testing functions that are located on one of the radiation boundaries, and $\mathbf{E}_1$ and $\mathbf{E}_2$ contain interactions between basis and testing functions that are both located on radiation boundaries. Each of these matrices has entries of the general form

$$I_{mn} = \iint_{\Gamma} \frac{1}{\mu_r} \nabla T_m \cdot \nabla B_n - k^2 \varepsilon_r T_m B_n \tag{7.170}$$

Submatrices $\mathbf{J}_1$ and $\mathbf{J}_2$ have entries

$$J_{1,mn} = -j\omega\mu_0 \int_{\partial\Gamma_1} T_m(t) B_n(t)\, dt \tag{7.171}$$

and

$$J_{2,mn} = -j\omega\mu_0 \int_{\partial\Gamma_2} T_m(t) B_n(t)\, dt \tag{7.172}$$

Since we have not yet incorporated the RBC or the incident field, (7.169) is underdetermined and has no driving function.

For the TM polarization, it is convenient to obtain an RBC from the EFIE

$$E_z^{\text{inc}}(t) = K_t(t) + jk\eta A_z(t) + \hat{z} \cdot \nabla \times \bar{F}_t|_{\partial\Gamma^+} \tag{7.173}$$

which can be used to relate the incident field and equivalent sources J_z and K_t along either $\partial\Gamma_1$ or $\partial\Gamma_2$. Repeating the procedure discussed in Section 7.10, we incorporate the Floquet condition in order to adapt (7.173) to the periodic geometry illustrated in Figures 7.16 and 7.17. Consequently, on either boundary,

$$A_z(t) = \int_{\text{one period}} J_z(t') G_p(x(t) - x(t'), 0)\, dt' \tag{7.174}$$

and

$$\bar{F}_t(t) = \int_{\text{one period}} \hat{t}(t') K_t(t') G_p(x(t) - x(t'), 0)\, dt' \tag{7.175}$$

where $\hat{t} = \hat{x}$ for points along $\partial\Gamma_1$, $\hat{t} = -\hat{x}$ for points along $\partial\Gamma_2$, and

$$G_p(x, y) = \frac{1}{4j} \sum_{q=-\infty}^{\infty} H_0^{(2)}\left[k\sqrt{(x - qa)^2 + y^2}\right] e^{-jqk_x a} \tag{7.176}$$

Using the expansion (7.168), the representation

$$K_t(t) \cong \sum_{n=1}^{M} e_n B_n(t) \tag{7.177}$$

(where B_n again denotes a subsectional triangle basis function), and point matching at the nodes of the mesh located along either radiation boundary, the EFIE in (7.173) can be discretized into the form

$$\mathbf{Aj} + \mathbf{Be} = \mathbf{e}^{\text{inc}} \tag{7.178}$$

In (7.178), the entries of $\mathbf{A}$ are given by

$$A_{mn} = jk\eta \int_{\partial\Gamma} B_n(t')G_p(x(t_m) - x(t'), 0)\, dt' \tag{7.179}$$

where k and η assume the values k_1 and η_1 for points along $\partial\Gamma_1$ and k_2 and η_2 for points along $\partial\Gamma_2$. For these basis functions, the entries of $\mathbf{B}$ are

$$B_{mn} = \begin{cases} \frac{1}{2} & m = n \\ 0 & \text{otherwise} \end{cases} \tag{7.180}$$

which follows from the usual limiting procedure (Chapter 2). Assuming that the excitation is incident from the lower ($y < 0$) region in Figure 7.16,

$$e_m^{\text{inc}} = \begin{cases} E_0 e^{-jk_1(x(t_m)\cos\theta + y(t_m)\sin\theta)} & \text{for points along } \partial\Gamma_1 \\ 0 & \text{for points along } \partial\Gamma_2 \end{cases} \tag{7.181}$$

Consequently, for the boundary $\partial\Gamma_1$ a numerical RBC can be expressed as

$$\mathbf{j}_1 = \mathbf{A}_1^{-1}\mathbf{e}_1^{\text{inc}} - \mathbf{A}_1^{-1}\mathbf{B}_1\mathbf{e}_1 \tag{7.182}$$

Along $\partial\Gamma_2$, we obtain the RBC

$$\mathbf{j}_2 = -\mathbf{A}_2^{-1}\mathbf{B}_2\mathbf{e}_2 \tag{7.183}$$

These constraints can be substituted into (7.169) to produce

$$\begin{bmatrix} \mathbf{I} & \mathbf{I}_1^T & \mathbf{I}_2^T \\ \mathbf{I}_1 & \mathbf{E}_1 - \mathbf{J}_1\mathbf{A}_1^{-1}\mathbf{B}_1 & \mathbf{0} \\ \mathbf{I}_2 & \mathbf{0} & \mathbf{E}_2 - \mathbf{J}_2\mathbf{A}_2^{-1}\mathbf{B}_2 \end{bmatrix} \begin{bmatrix} \mathbf{e}^{\text{int}} \\ \mathbf{e}_1 \\ \mathbf{e}_2 \end{bmatrix} = \begin{bmatrix} \mathbf{0} \\ -\mathbf{J}_1\mathbf{A}_1^{-1}\mathbf{e}_1^{\text{inc}} \\ \mathbf{0} \end{bmatrix} \tag{7.184}$$

Observe that blocks $\mathbf{I}$, $\mathbf{I}_1$, $\mathbf{I}_2$, $\mathbf{I}_1^T$, and $\mathbf{I}_2^T$ are sparse, while the remaining two blocks along the main diagonal are fully populated. Equation (7.184) is a properly determined system that can be solved for the coefficients $\{e_n\}$ of the interior basis functions. This system of equations constitutes an outward-looking formulation, as defined in Chapter 3, since the primary unknowns represent the interior fields.

We have described the formulation in general terms and now consider some of the details associated with evaluating the entries in (7.184). Consider the boundaries $\partial\Gamma_3$ and $\partial\Gamma_4$ as shown in Figure 7.17. The nodes located along $\partial\Gamma_4$ represent "dummy" values, since the fields on $\partial\Gamma_4$ are prescribed by the Floquet condition (7.162). Thus, there will be no unknowns (and no matrix rows or columns) associated with these nodes. Furthermore, in order to enforce the desired periodicity, each node on $\partial\Gamma_4$ must be the periodic translation of a corresponding node along $\partial\Gamma_3$. The matrix entries arising from the scalar Helmholtz equation can be constructed in the usual manner using the "element matrix" concept developed in Chapter 3. As a consequence of the Floquet condition, however, any element matrix entry involving a testing function located on $\partial\Gamma_4$ must be scaled by $e^{jk_x a}$ and added to the matrix row associated with the corresponding node along $\partial\Gamma_3$. Similarly, any element matrix entry involving a basis function on $\partial\Gamma_4$ must be scaled by $e^{-jk_x a}$ and added to the

matrix column associated with the corresponding node along $\partial\Gamma_3$. These operations force the fields to "wrap around" the unit cell in the desired periodic manner.

The entries of $\mathbf{J}_1$ and $\mathbf{J}_2$ also "wrap around" the unit cell. Consider the special case of N uniformly spaces nodes along $\partial\Gamma_1$, where $N+1$ denotes the index of the dummy node at the $\partial\Gamma_4$ corner. For subsectional triangle basis functions for J_z and piecewise-linear testing functions $\{T_m(t)\}$, the entries of $\mathbf{J}_1$ are given by

$$J_{1,mn} = -j\omega\mu_0 b \begin{cases} \frac{2}{3} & m = n \\ \frac{1}{6} & |m-n| = 1 \\ \frac{1}{6}e^{-jk_x a} & m = 1 \text{ and } n = N \\ \frac{1}{6}e^{jk_x a} & m = N \text{ and } n = 1 \end{cases} \tag{7.185}$$

The entries of $\mathbf{J}_2$ have a similar form.

Finally, again under the assumption of uniformly spaced nodes, the entries of $\mathbf{A}_1$ can be obtained along $\partial\Gamma_1$ as the inverse Fourier transform summation

$$A_{mn} = \frac{k_1\eta_1}{2a}\sum_{i=-\infty}^{\infty}\frac{\sin^2(\pi bf)}{b(\pi f)^2}\frac{e^{j2\pi f(x_m-x_n)}}{\beta_y}\Bigg]_{f=i/a-k_x/2\pi} \tag{7.186}$$

where a denotes the period, b denotes the uniform interval size, and β_y is defined in (7.45). A similar expression may be obtained for boundary $\partial\Gamma_2$. Observe that the ith term in (7.186) behaves as $O(i^{-3})$, ensuring convergence of the summation. We leave the generalization of this expression for nonuniformly spaced nodes as an exercise.

The numerical approach requires a scatterer model containing a list of node coordinates (x_i, y_i), a connectivity array linking cell indices to those of the surrounding nodes, and pointers to identify nodes on imbedded conducting boundaries as well as those located along $\partial\Gamma_1$, $\partial\Gamma_2$, and $\partial\Gamma_4$. An additional pointer is required to link the dummy nodes along $\partial\Gamma_4$ with their counterparts along $\partial\Gamma_3$. Finally, the usual arrays providing the material parameters of each cell are also necessary.

After Equation (7.184) is solved to produce the fields throughout the computational domain Γ, the fields along $\partial\Gamma_1$ and $\partial\Gamma_2$ are readily decomposed into a Floquet harmonic representation such as (7.21), where

$$e_n = \frac{1}{a}\int_0^a E_z(x, y_0)e^{jk_{xn}x}\,dx \tag{7.187}$$

and where k_{xn} is defined in Equation (7.23). The Floquet harmonic description is often useful for constructing scattering or transmission matrices, as discussed in Section 7.9.

The TE polarization can be obtained from the preceding expressions using the duality concept. To illustrate the performance of the procedure, we initially apply it to the corrugated surface depicted in Figure 7.14. Table 7.2 presents numerical values for the magnitudes of the Floquet harmonics in response to a TE-to-z illumination. Results from the outward-looking formulation of this section are compared with results from the coupled-wave formulation of reference [21], which were previously used to plot Figure 7.15. The numerical results were obtained using triangular-cell models with a maximum cell size of approximately $\lambda_0/20$. Excellent agreement is observed between the two procedures.

Figure 7.18 shows one period of an inhomogeneous structure consisting of a corrugated conducting region surrounded by a dielectric cladding. The response of the structure to normally incident TM and TE plane waves, obtained using the outward-looking formulation of this section, is displayed in Figures 7.19 and 7.20.

TABLE 7.2 Magnitude of nth Floquet Harmonic as a Function of Corrugation Depth d for Geometry Illustrated in Figure 7.14

Harmonic, n	Depth, d	Outward-Looking Approach	Coupled-Wave Approach
0 refl.	0.25	0.102	0.104
	0.5	0.017	0.017
	0.75	0.029	0.028
	1.0	0.009	0.008
1 refl.	0.25	0.135	0.134
	0.5	0.114	0.114
	0.75	0.052	0.048
	1.0	0.040	0.042
−1 trans.	0.25	0.306	0.308
	0.5	0.422	0.421
	0.75	0.403	0.396
	1.0	0.350	0.350
0 trans.	0.25	1.157	1.158
	0.5	1.113	1.115
	0.75	1.056	1.064
	1.0	0.983	0.987
1 trans.	0.25	0.167	0.168
	0.5	0.338	0.340
	0.75	0.503	0.495
	1.0	0.647	0.645

Note: Results obtained from the outward-looking formulation of this section (reconfigured for the TE-to-z polarization) are compared with results obtained from the "coupled-wave" approach of reference [21]. The depth is in λ.

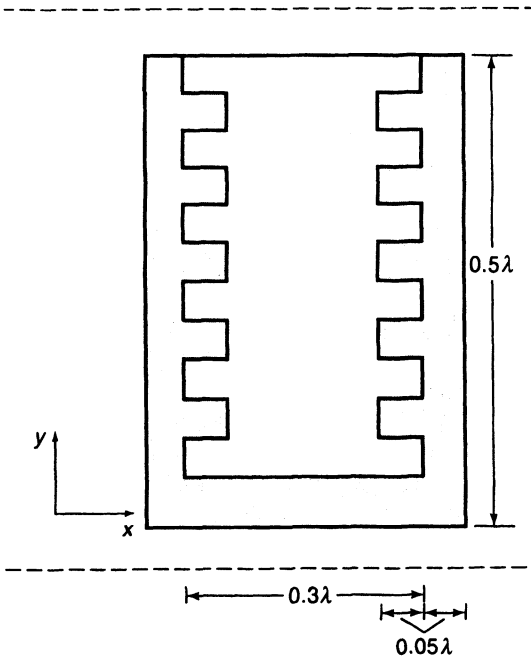

Figure 7.18 Corrugated p.e.c. cylinder partially coated with a lossless dielectric ($\epsilon_r = 3$). This structure comprises one element of an infinite periodic array along the x-axis. After [22]. ©1994 Taylor & Francis.

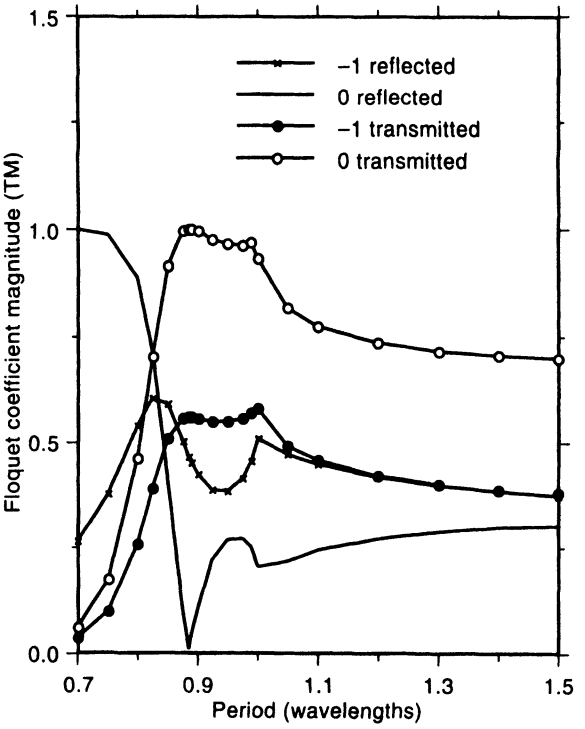

Figure 7.19 Response of the periodic array when illuminated by a TM-to-z wave propagating into the y direction. After [22]. ©1994 Taylor & Francis.

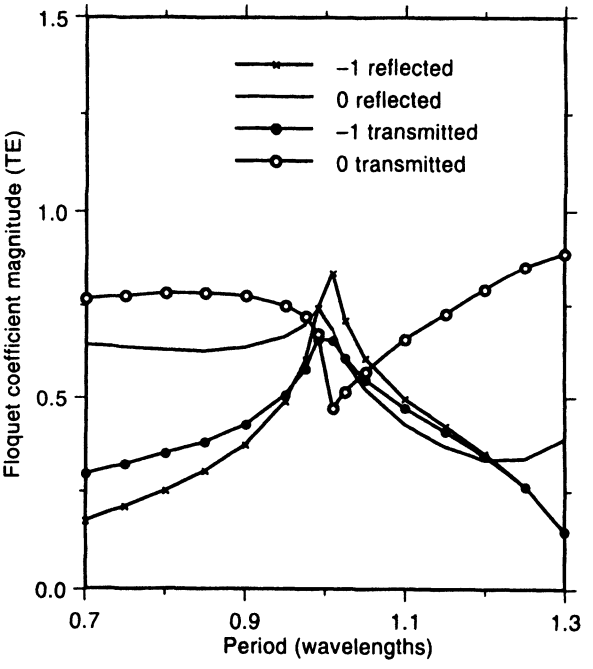

Figure 7.20 Response of the periodic array when illuminated by a TE-to-z wave propagating in the y direction. After [22]. ©1994 Taylor & Francis.

In this section, we have presented an outward-looking formulation for general two-dimensional structures having one-dimensional periodicity. We have also illustrated the use of an integral equation RBC. There are a variety of other ways in which integral and

differential equations can be combined into hybrid formulations for periodic structures, as attested to by the recent literature [23].

7.12 SUMMARY

This chapter has extended and applied the integral and differential equation formulations discussed in Chapters 2 and 3 to problems exhibiting one-dimensional periodicity. Because the required computational domain can be restricted to a single unit cell, these geometries are tractable despite their electrically large nature. However, the trade-off involves a Green's function that generally appears in the form of a slowly converging summation. Several acceleration procedures have been introduced to facilitate the required computations.

REFERENCES

[1] E. O. Brigham, *The Fast Fourier Transform and Its Applications*, Englewood Cliffs, NJ: Prentice-Hall, 1988.

[2] N. Amitay, V. Galindo, and C. P. Wu, *Theory and Analysis of Phased Array Antennas*, New York: Wiley, 1972.

[3] Y. T. Lo and S. W. Lee, "Affine transformation and its application to antenna arrays," *IEEE Trans. Antennas Propagat.*, vol. AP-13, pp. 890–896, Nov. 1965.

[4] R. E. Jorgenson, "Electromagnetic scattering from a structured slab comprised of periodically placed resistive cards," Ph.D. dissertation, University of Illinois, Urbana, IL, 1989.

[5] L. A. Weinstein, *The Theory of Diffraction and the Factorization Method*, Boulder, CO: Golem, 1969, pp. 267–290.

[6] T. A. Cwik, "Scattering from general periodic surfaces," Ph.D. dissertation, University of Illinois, Urbana, IL, 1986.

[7] R. Lampe, P. Klock, and P. Mayes, "Integral transforms useful for the accelerated summation of periodic, free-space Green's functions," *IEEE Trans. Microwave Theory Tech.*, vol. MTT-33, pp. 734–736, Aug. 1985.

[8] R. E. Jorgenson and R. Mittra, "Efficient calculation of the free-space periodic Green's function," *IEEE Trans. Antennas Propagat.*, vol. AP-38, pp. 633–642, May 1990.

[9] S. Singh, W. F. Richards, J. R. Zinecker, and D. R. Wilton, "Accelerating the convergence of series representing the free space periodic Green's function," *IEEE Trans. Antennas Propagat.*, vol. AP-38, pp. 1958–1962, Dec. 1990.

[10] M. E. Veysoglu, "Polarimetric passive remote sensing of periodic surfaces and anisotropic media," M.S. Thesis, Massachusetts Institute of Technology, Cambridge, MA, May 1991.

[11] I. S. Gradshteyn and I. M. Ryzhik, *Table of Integrals, Series, and Products*, New York: Academic, 1980.

[12] K. E. Jordan, G. R. Richter, and P. Sheng, "An efficient numerical evaluation of the Green's function for the Helmholtz operator on periodic surfaces," *J. Computat. Phys.*, vol. 63, pp. 222–235, 1986.

[13] P. P. Ewald, "Die berechnung optischer und elektrostatischen giterpotentiale," *Ann. der Phys.*, vol. 64, p. 253, 1921.

[14] A. W. Mathis and A. F. Peterson, "A comparison of acceleration procedures for the two-dimensional periodic Green's function," *IEEE Trans. Antennas Propagat.*, vol. 44, pp. 567–571, Apr. 1996.

[15] T. Cwik and R. Mittra, "The cascade connection of planar periodic surfaces and lossy dielectric layers to form an arbitrary periodic screen," *IEEE Trans. Antennas Propagat.*, vol. AP-35, pp. 1397–1405, Dec. 1987.

[16] R. C. Hall, R. Mittra, and K. M. Mitzner, "Analysis of multilayered periodic structures using generalized scattering matrix theory," *IEEE Trans. Antennas Propagat.*, vol. AP-36, pp. 511–517, Apr. 1988.

[17] R. E. Collin, *Foundations for Microwave Engineering*, New York: McGraw-Hill, 1966.

[18] R. Mittra and S. W. Lee, *Analytical Techniques in the Theory of Guided Waves*, New York: Macmillan, 1971, pp. 207–211.

[19] T. Itoh, "Generalized scattering matrix technique," in *Numerical Techniques for Microwave and Millimeter-Wave Passive Structures*, ed. T. Itoh, New York: Wiley, 1989.

[20] A. F. Peterson, "Integral equation formulation for scattering from continuous or discrete dielectric targets exhibiting one-dimensional periodicity," *Arch. Elektron. Uebertragungst.*, vol. 46, pp. 336–342, Sept. 1992.

[21] M. G. Moharam and T. K. Gaylord, "Diffraction analysis of dielectric surface-relief gratings," *J. Opt. Soc. Am.*, vol. 72, pp. 1385–1392, 1982.

[22] A. F. Peterson, "An outward-looking differential equation formulation for scattering from one-dimensional periodic diffraction gratings," *Electromagnetics*, vol. 14, pp. 227–238, 1994.

[23] S. D. Gedney, J. F. Lee, and R. Mittra, "A combined FEM/MoM approach to analyze the plane wave diffraction by arbitrary gratings," *IEEE Trans. Antennas Propagat.*, vol. 40, pp. 363–370, Feb. 1992.

PROBLEMS

P7.1 (a) Using the Fourier transform of the comb function $P(x)$ defined in (7.9), derive the relationship

$$\sum_{n=-\infty}^{\infty} e^{-j2\pi nf/\Delta f} = \Delta f \sum_{n=-\infty}^{\infty} \delta(f - n\Delta f)$$

(b) By considering the Fourier transform of the product $U(x)P(x)$, where U is arbitrary and P is the comb function used in part (a), derive the *Poisson summation formula*

$$\sum_{n=-\infty}^{\infty} U(n\Delta X) = \frac{1}{\Delta X} \sum_{n=-\infty}^{\infty} \tilde{U}\left(\frac{n}{\Delta X}\right)$$

P7.2 If $\tilde{U}(f)$ is the Fourier transform of $U(x)$ according to the definition in (7.1), show that the Fourier transform of

$$U(x)e^{j2\pi f_0 x}$$

is given by $\tilde{U}(f - f_0)$.

P7.3 Identify the propagating Floquet harmonics for a strip grating with period equal to 3λ and a wave incident from an angle 45° normal to the grating. Provide a sketch similar to Figure 7.4 showing the direction of each propagating harmonic.

P7.4 A two-dimensional periodic surface is defined by the spatial lattice $x = m\Delta X$ and $y = n\Delta Y$. The excitation imposes a phase shift of $k_x \Delta X$ from one cell to another in the x direction and $k_y \Delta Y$ from one cell to another along y.

(a) Identify the values of f and g that comprise the reciprocal lattice (the discrete spectral frequencies associated with the Floquet harmonics).

(b) If $\Delta X = 0.1\lambda$, $\Delta Y = 0.5\lambda$, and the excitation is a plane wave incident at an angle 45° from normal along x and 45° from normal along y, identify the propagating Floquet harmonics.

P7.5 For the TM-to-z representation given in (7.21), show that the time-averaged power per period carried by the nth propagating Floquet harmonic in the y direction is

$$\frac{a|e_n|^2}{2k\eta}\sqrt{k^2 - k_{xn}^2}$$

assuming that the phasor representation for E_z is based on peak value rather than root-mean-square (rms) value.

P7.6 Consider the strip grating of Figure 7.3 illuminated by a TE-to-z plane wave that excites a current density J_x on the conducting strips. The scattered field can be expressed as

$$H_z^s(x, y) = \begin{cases} \displaystyle\sum_{n=-\infty}^{\infty} h_n^+ e^{-jk_{xn}x} e^{-j\sqrt{k^2 - k_{xn}^2}\,y} & y > 0 \\ \displaystyle\sum_{n=-\infty}^{\infty} h_n^- e^{-jk_{xn}x} e^{j\sqrt{k^2 - k_{xn}^2}\,y} & y < 0 \end{cases}$$

where k_{xn} is defined in (7.23). Find an expression for the coefficients h_n^+ and h_n^- in terms of the current density $J_x(x)$.

P7.7 (a) Using $G_p(x)$ and $G_a(x)$ defined in (7.32) and (7.50), respectively, and the asymptotic form of the Hankel function from (7.42), show that the magnitude of the nth term in the difference summation $G_p(x) - G_a(x)$ tends to

$$\left(\frac{\alpha}{a}\right)^2 n^{-3/2}\sqrt{\frac{ka}{32\pi}} \qquad \text{as } n \to \infty.$$

Hint: Use the approximation

$$\sqrt{(na - x)^2 + \alpha^2} \cong (na - x)\sqrt{1 + \frac{\alpha^2}{(na)^2}} \cong (na - x)\left(1 + \frac{\alpha^2}{2(na)^2}\right)$$

(b) An alternative expression for the periodic Green's function is

$$G_p(x) = G_b(x) + F^{-1}\{\tilde{G}_p(f) - \tilde{G}_b(f)\}$$

where $\tilde{G}_p(f)$ is defined in Equation (7.46) and $\tilde{G}_b(f)$ is defined in (7.63). Use techniques similar to those employed in part (a) to show that the nth term in the difference summation $F^{-1}\{\tilde{G}_p(f) - \tilde{G}_b(f)\}$ is $O(n^{-3})$ as $n \to \infty$.

P7.8 Using (1.46) and (7.44), evaluate the two-dimensional Fourier transform of the three-dimensional free-space Green's function to produce

$$\int_{-\infty}^{\infty}\int_{-\infty}^{\infty} \frac{e^{-jk\sqrt{x^2+y^2}}}{4\pi\sqrt{x^2 + y^2}} e^{-j2\pi fx} e^{-j2\pi gy}\, dx\, dy = \frac{1}{j2\beta_z}$$

where

$$\beta_z = \begin{cases} \sqrt{k^2 - (2\pi f)^2 - (2\pi g)^2} & k^2 > (2\pi f)^2 + (2\pi g)^2 \\ -j\sqrt{(2\pi f)^2 + (2\pi g)^2 - k^2} & \text{otherwise} \end{cases}$$

P7.9 The three-dimensional Green's function describing the potential on a planar surface having a regular two-dimensional periodicity can be expressed in the spatial domain as

$$G_p(x - x', y - y') = \sum_{m=-\infty}^{\infty} \sum_{n=-\infty}^{\infty} \frac{e^{-jkR_{mn}}}{4\pi R_{mn}} e^{-jmk_x a} e^{-jnk_y b}$$

where

$$R_{mn} = \sqrt{(x - x' - ma)^2 + (y - y' - nb)^2}$$

(a) Identify the asymptotic order of the (mn)th term in the summation.

(b) Using the result of Prob. P7.8 and properties of the Fourier transform, show that an equivalent summation is given by

$$G_p(x - x', y - y') = \frac{1}{ab} \sum_{m=-\infty}^{\infty} \sum_{n=-\infty}^{\infty} \frac{1}{j2\beta_z} e^{j2\pi f(x-x')} e^{j2\pi g(y-y')} \Bigg]_{f=m/a-k_x/2\pi, g=n/b-k_y/2\pi}$$

where β_z is defined in Prob. P7.8.

(c) What is the asymptotic order of the (mn)th term in the new summation?

P7.10 (a) Using the idea expressed in Equation (7.49), develop an alternative procedure for computing the three-dimensional periodic Green's function defined in Prob. P7.9. Determine the asymptotic order of the (mn)th term in each of the new summations.

(b) Using the idea expressed in Prob. P7.7(b), develop a different procedure for computing the three-dimensional periodic Green's function, and determine the asymptotic order of the (mn)th term in each of the new summations.

P7.11 Suppose that the TM strip grating formulation in Section 7.3 is posed using pulse testing functions instead of Dirac delta testing functions. Develop an expression for Z_{mn} analogous to (7.57) reflecting the change. What is the asymptotic behavior of the ith term in the new summation?

P7.12 Create a computer program to determine the surface current density and the reflection and transmission coefficients for a planar strip grating of perfect conductors illuminated by a TE-to-z plane wave. Develop a formulation along the lines of Section 7.7 (without including the dielectric slab support). Use subsectional triangle basis functions and subsectional pulse testing functions within a method-of-moments discretization. Implement a series acceleration technique similar to that Equation (7.115) to compute the matrix entries, placing all of the weight on the inverse Fourier transform summation.

P7.13 Develop a formulation for TM-to-z scattering from a strip grating backed by a dielectric slab. Using the discussion in Section 7.7 as a guide, find the appropriate TM Green's function for a line source radiating on the surface of a slab, construct an EFIE expressed as an integral over a single strip, and identify matrix entries associated with a pulse basis function and Dirac delta testing function discretization. Write the matrix entries in the form of an inverse Fourier transform summation, similar to (7.115).

P7.14 Using the Green's function in Equation (7.107) for a TE line source radiating on the surface of a dielectric slab, develop an EFIE formulation for TE scattering from a single conducting strip on the surface of a dielectric slab. Provide expressions for the matrix entries associated with subsectional triangle basis and pulse testing functions. Discuss ways in which you might evaluate the matrix entries. Equation (7.107) is one form of a Sommerfeld integral, and a number of special procedures have been developed for its efficient evaluation.

P7.15 The planar strip grating geometries discussed in Sections 7.3, 7.7, and 7.8 are easily adapted to iterative solution procedures such as the CG–FFT approach from Chapter 4. For the TM grating formulation in Section 7.3, describe the specialization necessary to produce (7.33) in a form suitable for CG–FFT solution.

P7.16 For the aperture formulation of Section 7.8, find an expression for the coefficients of the Floquet harmonics in terms of the aperture field $E_z(x)$.

P7.17 Develop an integral equation formulation to treat TM-to-z scattering from a one-dimensional periodic array of homogeneous dielectric scatterers, where the unit cell consists of a single scatterer of general shape. Use a coupled EFIE formulation, with the exterior equation (Section 7.10) incorporating periodicity in the x direction. The interior equation does not involve a periodic Green's function and may be found in Section 2.8. Provide the equations, and develop (nonaccelerated) expressions for the matrix entries associated with pulse basis functions and Dirac delta testing functions.

P7.18 Using the TM formulation in Section 7.11 as a guide, develop an outward-looking TE-to-z formulation for scattering from an inhomogeneous grating exhibiting periodicity in the x direction. Develop RBCs from a discretization of the MFIE, and define all entries of the global finite-element matrix, assuming the use of linear interpolation functions on triangular cells.

P7.19 The Floquet expansion discussed in Section 7.2 can be used to develop an alternate RBC that can replace the integral equation RBC employed in Section 7.11. By expanding $E_z(x, y)$ in a Floquet expansion, use a development similar to that of Section 3.3 in order to obtain the RBC

$$\frac{\partial E_z^s}{\partial y} = \frac{1}{a}\int_0^a E_z^s(x', y)G(x - x', y)\,dx'$$

applicable along boundary $\partial\Gamma_2$ in Figure 7.17, where

$$G(x, y) = -j\sum_{n=-\infty}^{\infty}\sqrt{k^2 - k_{xn}^2}\,e^{-jk_{xn}x}e^{-j\sqrt{k^2-k_{xn}^2}\,y}$$

and k denotes the wavenumber of region 2. Find a similar expression for an RBC applicable to points along boundary $\partial\Gamma_1$ in Figure 7.17. Is there a connection between this RBC and the integral equation RBC used in Section 7.11?